






Loss of BRD4 induces cell senescence in HSC/HPCs by deregulating histone H3 clipping

Hui Yang^{1,†}, Pinpin Sui^{1,†} , Ying Guo^{1,†}, Shi Chen², Marie E Maloo³ , Guo Ge¹ , Francine Nihozeko¹ , Caroline R Delma⁴ , Ganqian Zhu², Peng Zhang¹ , Zhenqing Ye^{5,6}, Edward A Medina⁴ , Nagi G Ayad⁷, Ruben Mesa⁸, Stephen D Nimer³, Cheng-Ming Chiang^{9,10,11} , Mingjiang Xu^{2,8}, Yidong Chen^{5,6} & Feng-Chun Yang^{1,8,*} 

Abstract

Bromodomain-containing protein 4 (BRD4) is overexpressed and functionally implicated in various myeloid malignancies. However, the role of BRD4 in normal hematopoiesis remains largely unknown. Here, utilizing an inducible *Brd4* knockout mouse model, we find that deletion of *Brd4* (*Brd4*^{Δ/Δ}) in the hematopoietic system impairs hematopoietic stem cell (HSC) self-renewal and differentiation, which associates with cell cycle arrest and senescence. ATAC-seq analysis shows increased chromatin accessibility in *Brd4*^{Δ/Δ} hematopoietic stem/progenitor cells (HSC/HPCs). Genome-wide mapping with cleavage under target and release using nuclease (CUT&RUN) assays demonstrate that increased global enrichment of H3K122ac and H3K4me3 in *Brd4*^{Δ/Δ} HSC/HPCs is associated with the upregulation of senescence-specific genes. Interestingly, *Brd4* deletion increases clipped H3 (cH3) which correlates with the upregulation of senescence-specific genes and results in a higher frequency of senescent HSC/HPCs. Re-expression of BRD4 reduces cH3 levels and rescues the senescence rate in *Brd4*^{Δ/Δ} HSC/HPCs. This study unveils an important role of BRD4 in HSC/HPC function by preventing H3 clipping and suppressing senescence gene expression.

Keywords *Brd4*; hematopoiesis; histone clipping; senescence

Subject Categories Transcription & Genomics; Haematology; Stem Cells & Regenerative Medicine

DOI 10.15252/embr.202357032 | Received 17 February 2023 | Revised 28 July 2023 | Accepted 10 August 2023 | Published online 31 August 2023

EMBO Reports (2023) 24: e57032

See also: [N Dasgupta & PD Adams](#) (October 2023)

Introduction

Epigenetic regulators are a set of proteins that regulate gene transcription as writers, readers, or erasers of post-translational modifications on histone or non-histone proteins (Filippakopoulos & Knapp, 2014). Histone acetylation represents a major epigenetic hallmark for open chromatin and transcriptional activation (Struhl, 1998). Bromodomain-containing protein 4 (BRD4) is one of the bromodomain and extra-terminal (BET) family members that utilize tandem bromodomain (BRD) modules to recognize and dock themselves onto acetylated lysines (Dey *et al*, 2000; Zeng & Zhou, 2002; Yang *et al*, 2005; Chiang, 2009). BRD4 involves in transcription activation and elongation through the recruitment of the P-TEFb complex and many other transcription factors (Jang *et al*, 2005; Yang *et al*, 2005; Wu & Chiang, 2007; Wu *et al*, 2013; Shi & Vakoc, 2014). BRD4 also functions as a histone acetyltransferase, which made it an attractive therapeutic target for cancers.

BRD4 is overexpressed and functionally deregulated in diverse solid tumors and hematologic malignancies, such as lymphoma and myeloid malignancies (Bansal *et al*, 2017; Lee *et al*, 2018; Ozer *et al*, 2018; Lu *et al*, 2020). Small-molecule inhibitors directed toward the acetyl-lysine binding bromodomain have been developed, such as the prototypical JQ1 (Filippakopoulos *et al*, 2010). Inhibition of BRD4 shows great promise in treating MYC-driven cancers (Delmore *et al*, 2011; Mertz *et al*, 2011). As a proof of concept, knockdown of BRD4 inhibits the proliferation of MLL-AF9 leukemic cells (Zuber *et al*, 2011). To date, BET inhibitors (BETi) are effective *in vitro* and *in vivo* against various mouse models of hematological malignancies, including myeloid leukemia and lymphoma

1 Department of Cell Systems and Anatomy, University of Texas Health San Antonio, San Antonio, TX, USA

2 Department of Molecular Medicine, University of Texas Health San Antonio, San Antonio, TX, USA

3 Sylvester Comprehensive Cancer Center, University of Miami Miller School of Medicine, Miami, FL, USA

4 Department of Pathology and Laboratory Medicine, Division of Hematopathology, University of Texas Health San Antonio, San Antonio, TX, USA

5 Department of Population Health Sciences, University of Texas Health San Antonio, San Antonio, TX, USA

6 Greehey Children's Cancer Research Institute, University of Texas Health San Antonio, San Antonio, TX, USA

7 Department of Oncology, Lombardi Comprehensive Cancer Center, Georgetown University, Washington, DC, USA

8 Mays Cancer Center, University of Texas Health San Antonio, San Antonio, TX, USA

9 Simmons Comprehensive Cancer Center, University of Texas Southwestern Medical Center, Dallas, TX, USA

10 Department of Biochemistry, University of Texas Southwestern Medical Center, Dallas, TX, USA

11 Department of Pharmacology, University of Texas Southwestern Medical Center, Dallas, TX, USA

*Corresponding author. Tel: +1 210 450 8069; E-mail: yangf1@uthscsa.edu

†These authors contributed equally to this work

(Dawson *et al*, 2011; Wang & Filippakopoulos, 2015; Amorim *et al*, 2016; Berthon *et al*, 2016).

Deletion of *Brd4* in the thymus via *Lck-Cre* showed that BRD4 is critical for normal T cell development (Gegonne *et al*, 2018). Dey *et al* (2019) recently reported that BRD4 modulates macrophage inflammatory responses, and *Vav-Cre*-based *Brd4* deletion blocks fetal liver hematopoietic stem cell (HSC) development. These results demonstrate an important role of BRD4 in fetal liver HSC and T cell development, as well as immune response. Despite the clinical significance of BRD4 in various hematological malignancies, the role and the underlying mechanisms of BRD4 in regulating HSC/HPC functions remain largely unknown.

Here, we used an inducible *Brd4* knockout mouse model aiming to uncover undefined roles of BRD4 in hematopoietic stem cells. We found that loss of *Brd4* led to robust senescence in HSC/HPCs and severe functional impairments, such as stem cell self-renewal and biased lineage commitment toward myeloid cells. Mechanistically, *Brd4* deletion increases chromatin accessibility by enhancing H3K122ac, H3K4me3, and H3K27ac occupancies at senescence-related gene loci. Intriguingly, the deletion of *Brd4* in HSC/HPCs induces H3 clipping (cH3). The proteolytic cleavage of histone H3 N-terminal tail (H3 clipping) happens during several cellular processes, including cellular differentiation (Duncan *et al*, 2008), cellular senescence (Duarte *et al*, 2014), osteoclastogenesis (Kim *et al*, 2016), and monocyte-to-macrophage differentiation (Cheung *et al*, 2021). Using CUT&RUN analysis, we found that cH3 enrichment is highly associated with chromatin accessibility and senescence-related gene expression. Our study demonstrates an essential role of BRD4 in normal hematopoietic stem cell functions by maintaining normal chromatin structure, preventing H3 clipping, and repressing senescence gene expression, thereby sustaining proper HSC/HPC functions.

Results

Brd4 is required for normal adult hematopoiesis

To determine *Brd4* expression over the course of HSC commitment and differentiation, we sorted different HSC/HPC subpopulations from the bone marrow (BM) of wild-type (WT) mice. Quantitative real-time PCR (qPCR) analysis showed that *Brd4* expression levels are higher in HSCs and progenitors, but lower in mature myeloid lineages (Appendix Fig S1A). To decipher the role of BRD4 in adult HSC/HPC functions *in vivo*, we generated *Brd4^{fl/fl}; Mx1Cre⁺* mice and injected polyinosinic:polycytidylic (*pl:pC*) to induce *Brd4* deletion (*Brd4^{Δ/Δ}*) in the hematopoietic system (Appendix Fig S1B). *Mx1 Cre⁺*-only mice were used as WT control. BRD4 protein expression was not detected in *Brd4^{Δ/Δ}* BM cells 1 week after *pl:pC* injection (Appendix Fig S1C). Although the appearance and body weights of the *Brd4^{Δ/Δ}* mice were similar to WT and *Brd4^{Δ/+}* mice (Fig EV1A and B), all of the *Brd4^{Δ/Δ}* mice died around 3 weeks after *pl:pC* injection (Fig 1A). To determine the impact of *Brd4* deletion on adult hematopoiesis, we performed the phenotypic analysis of hematopoietic organs of WT, *Brd4^{Δ/+}*, and *Brd4^{Δ/Δ}* mice 2 weeks after *pl:pC* injection. Peripheral blood (PB) counts showed significantly lower levels/counts of hemoglobin (Hb), red blood cells (RBC), and platelets (PLT) in *Brd4^{Δ/Δ}* mice compared to WT and

Brd4^{Δ/+} mice (Fig 1B–D). No significant changes were observed in the number of white blood cells (WBC), neutrophils (NE), or monocytes (MO) in the PB of *Brd4^{Δ/Δ}* mice compared to the WT mice (Fig EV1C).

Further phenotypic characterization of the mice revealed that the femurs of the *Brd4^{Δ/Δ}* mice were pale and *Brd4^{Δ/Δ}* BM cellularity was significantly lower than that of WT and *Brd4^{Δ/+}* mice (Fig 1E and F). Histologic analysis of femur sections and cytospin preparations of BM cells revealed dramatically less erythroid islands and more immature myeloid cells in the BM of *Brd4^{Δ/Δ}* mice compared to WT mice (Fig 1G and H). Consistently, the ratio of myeloid cells to nucleated erythroid cells (M/E) in *Brd4^{Δ/Δ}* BM cells was increased compared to WT BM cells (Fig EV1D). Flow cytometry analysis showed a drastic reduction in the frequencies of erythroid cell populations (Ter119⁺/CD71⁺ and Ter119⁺/CD71⁻) in *Brd4^{Δ/Δ}* BM compared to WT BM (Fig 1I). There was a shift of lineage toward the myeloid cell population from Gr1⁺/Mac1⁺ to Gr1⁻/Mac1⁺ cells in *Brd4^{Δ/Δ}* BM cells (Fig 1J and K), away from the B cell population (B220⁺/IgM⁺ and B220⁻/IgM⁺) in *Brd4^{Δ/Δ}* BM cells compared to WT BM cells (Fig EV1E). While the spleen weights of *Brd4^{Δ/Δ}* mice were lower than that of WT and *Brd4^{Δ/+}* mice, the spleen cellularity of *Brd4^{Δ/Δ}* mice was similar to that of WT and *Brd4^{Δ/+}* mice (Fig EV1F and G). Histologic analyses of spleen sections showed lack of matured erythroid cells in the *Brd4^{Δ/Δ}* section than the WT section (Fig EV1H). Collectively, these data indicate that *Brd4* is required for normal adult hematopoiesis in mice.

Deletion of *Brd4* alters hematopoietic stem cell function

To determine whether deletion of *Brd4* affects the HSC/HPC pool *in vivo*, we performed flow cytometry analysis to assess the subpopulation of HSC/HPCs in the BM of WT, *Brd4^{Δ/+}*, and *Brd4^{Δ/Δ}* mice. Strikingly, we observed a dramatic increase in the frequency of Lin⁻ (lineage-negative) population in *Brd4^{Δ/Δ}* compared to WT and *Brd4^{Δ/+}* BM (Figs 2A and EV1I). Further analysis of the subpopulations of HSC/HSPCs revealed a significant increase in the frequencies of LKS⁻ (Lin⁻ckit⁺Scal1⁻), common myeloid progenitor (CMP, LKS⁻CD34⁺CD16/32⁻), granulocyte/macrophage progenitor (GMP, LKS⁻CD34⁺CD16/32⁺), and megakaryocyte–erythroid progenitor (MEP, LKS⁻CD34^{low}CD16/CD32^{low}) populations in the BM of *Brd4^{Δ/Δ}* mice compared to WT and *Brd4^{Δ/+}* mice (Appendix Fig S1D). Additionally, a significant increase in frequencies of LSK and short-term HSCs (ST-HSCs, LSKCD135⁻CD34⁺) cell populations was also observed in the BM of *Brd4^{Δ/Δ}* mice compared to WT and *Brd4^{Δ/+}* mice (Appendix Fig S1E), while there were no significant changes in long-term HSCs (LT-HSCs, LSKCD135⁻CD34⁻) and multipotent progenitors (MPP, LSKCD135⁺CD34⁺) populations in the BM of *Brd4^{Δ/Δ}* mice compared to WT mice (Appendix Fig S1E). Interestingly, even though the BM cellularity is lower in *Brd4^{Δ/Δ}* mice (Fig 1F), the absolute numbers of Lin⁻, LKS⁻, CMP, and ST-HSC (Fig 2B and C) are still significantly increased in *Brd4^{Δ/Δ}* mice than in WT mice.

To evaluate the colony-forming ability of *Brd4^{Δ/Δ}* HSC/HPCs, we performed CFU-C assays with semisolid methylcellulose cultures using BM mononuclear cells (BMMNCs) of WT and *Brd4^{Δ/Δ}* mice. *Brd4^{Δ/Δ}* BM cells gave rise to a significantly lower number of CFU-Cs and these CFU-Cs were much smaller than those derived from WT BM cells (Figs 2D and EV1J). To further assess the

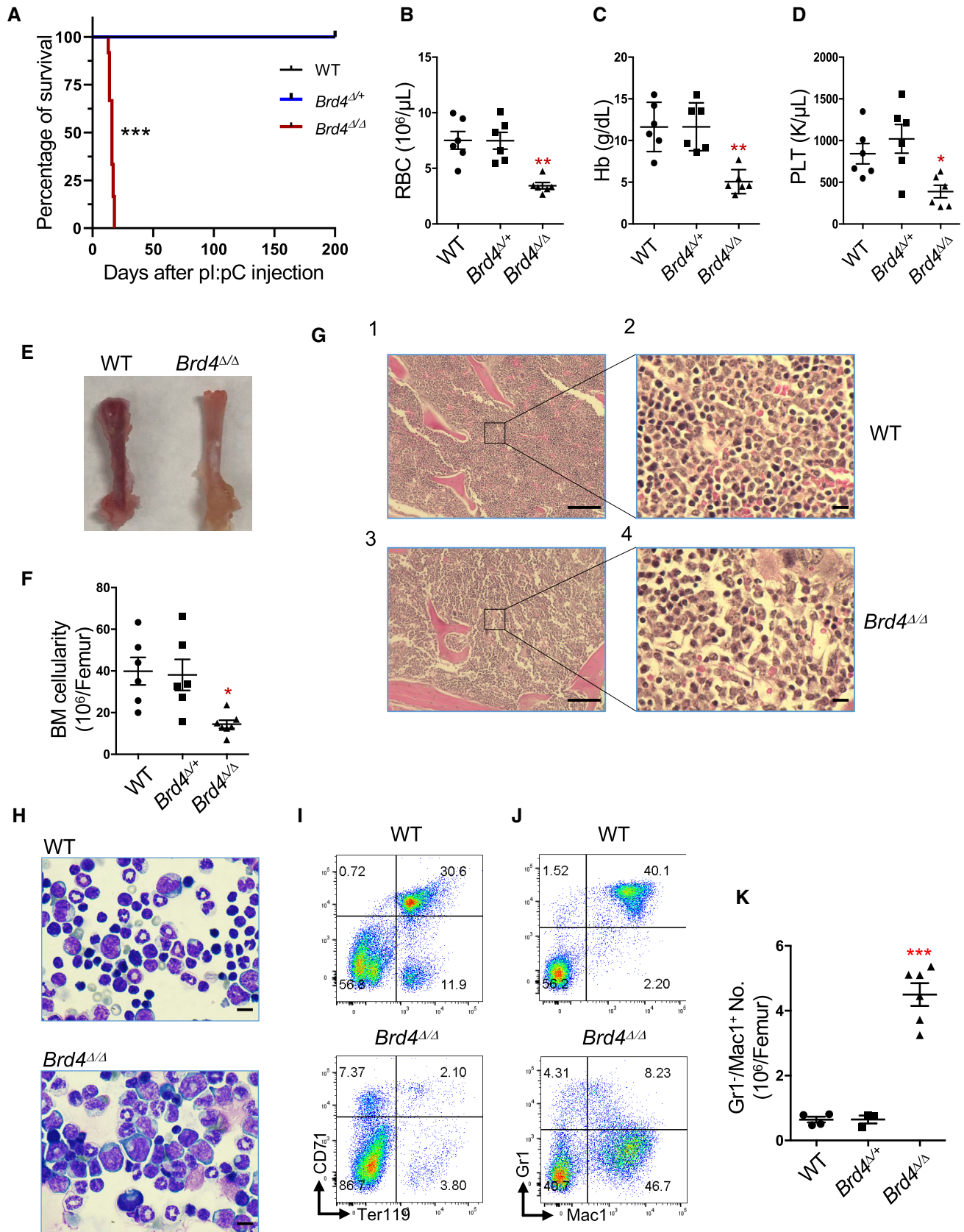


Figure 1.

Figure 1. Induced deletion of *Brd4* in adult bone marrow results in anemia and blockage of differentiation.

- A Kaplan–Meier survival curve representing percentage survival of *Brd4*^{Δ/Δ} mice after poly (I: C) injection. Log-rank (Mantel–Cox) test; WT, *n* = 12; *Brd4*^{Δ/+}, *n* = 12; *Brd4*^{Δ/Δ}, *n* = 12, *P* < 0.0001.
- B–D Peripheral blood (PB) counts of RBC (B) (WT vs. *Brd4*^{Δ/Δ}, *P* = 0.0026), Hb (C) (WT vs. *Brd4*^{Δ/Δ}, *P* = 0.0016), and PLT (D) (WT vs. *Brd4*^{Δ/Δ}, *P* = 0.0127) in WT, *Brd4*^{Δ/+}, and *Brd4*^{Δ/Δ} mice (*n* = 6 per genotype).
- E Representative bone marrow from WT and *Brd4*^{Δ/Δ} mice.
- F Bone marrow cellularity of WT, *Brd4*^{Δ/+}, and *Brd4*^{Δ/Δ} mice (*n* = 6 per genotype) (WT vs. *Brd4*^{Δ/Δ}, *P* = 0.01).
- G Hematoxylin and eosin (H&E)-stained sections of femurs from representative WT and *Brd4*^{Δ/Δ} mice (14 days after poly (I: C) injection). Scale bar, 1 mm (Left), 10 μm (Right).
- H Representative of May–Giemsa-stained BM cytopins prepared from WT and *Brd4*^{Δ/Δ} mice. Scale bar, 100 μm.
- I Flow cytometric analysis of erythroid cells in BM from WT and *Brd4*^{Δ/Δ} mice 14 days after first poly (I: C) injection.
- J Flow cytometric analysis of myeloid cells in BM from WT and *Brd4*^{Δ/Δ} mice 14 days after first poly (I: C) injection.
- K Frequency of Gr1[−]/Mac1⁺ cells in BM from WT and *Brd4*^{Δ/Δ} mice (WT, *n* = 4; *Brd4*^{Δ/+}, *n* = 3; *Brd4*^{Δ/Δ}, *n* = 6) (WT vs. *Brd4*^{Δ/Δ}, *P* < 0.0001) is shown.
- Data information: Data are shown as the Mean ± S.E.M. Comparisons among the groups were formed by one-way ANOVA. **P* < 0.05 ***P* < 0.01, ****P* < 0.001. Source data are available online for this figure.

colony-forming activity of *Brd4*^{Δ/Δ} HSCs, we sorted LT-HSCs and subjected them to CFU-C assays. *Brd4*^{Δ/Δ} LT-HSCs had limited colony-forming capacity (Fig 2E). To determine the proliferative potential of multipotent progenitor cells, we performed high proliferative potential colony-forming cell (HPP-CFC) assays on BMMNCs using double-layer agar cultures. While there was a substantial number of HPP-CFCs in WT cultures, HPP-CFCs were hardly detected in *Brd4*^{Δ/Δ} cultures (Fig EV1K). Consistently, serial replating assays demonstrated a profound reduction in CFU-Cs in the first and second replating, and no CFU-Cs were detected in the third replating in *Brd4*^{Δ/Δ} cultures compared to WT cultures (Fig 2F). These data indicate that although *Brd4* loss did not affect the pools of the HSC/HPCs in the BM, *Brd4* deletion diminishes HSC self-renewal.

To further determine the effects of *Brd4* loss on HSC/HPC self-renewal and repopulation capacity, we performed competitive transplantation assays to compare the repopulation capacity between WT and *Brd4*^{Δ/Δ} BM cells (at 1:1 ratio for donor vs. competitor cells). The *pl:pC* was injected into donor mice 2 weeks after transplantation to induce the deletion of *Brd4*. The donor cell chimerism was analyzed by flow cytometry on the PB of the recipient mice every other week. While the donor cell population (CD45.2⁺) remained at about 50% in the recipient mice receiving WT and *Brd4*^{Δ/Δ} BM cells right after the *pl:pC* injection (Fig 3A and B), CD45.2⁺ cells steeply declined in the PB of *Brd4*^{Δ/Δ} BM-transplanted recipients within the first 2 weeks and disappeared after 8 weeks (Fig 3B). A significant decrease in *Brd4*^{Δ/Δ}-derived chimerism within the BM of recipient mice was also observed (Appendix Fig S1F and G). These results indicate that *Brd4* loss-associated impairment in HSC/HPC function is cell autonomous.

Defective *Brd4*^{Δ/Δ} HSC/HPC function is associated with cell cycle arrest and increased senescence

To identify cell-intrinsic causes for the dysfunction of *Brd4*^{Δ/Δ} HSC/HPCs, we next compared the expansion, apoptosis, and mitotic status of WT and *Brd4*^{Δ/Δ} LK cells following the liquid culture containing a cocktail of growth factors (m-SCF, IL3, GM-CSF, EPO, and TPO). While the cell number in WT cell cultures continuously increased, the cell number in *Brd4*^{Δ/Δ} cultures remained at very low levels (Fig 3C). On day 7 of the culture, most of the cells in the WT cultures were Gr1⁺/Mac1⁺ (65%) and Gr1[−]/Mac1⁺ (21%) by flow cytometric analysis. By contrast, Gr1⁺/Mac1⁺ cells were only 32% and Gr1[−]/Mac1⁺ cells 41% in the *Brd4*^{Δ/Δ} cell cultures (Fig 3D). In addition, a significant reduction in the cells in the S-phase and a dramatically higher percentage of G0/G1 cells were observed in *Brd4*^{Δ/Δ} HSC/HPC cultures compared to WT cultures by BrdU incorporation assay followed by flow cytometry analysis (Figs 3E and EV2A). In contrast, the percentage of apoptotic cells was similar between WT and *Brd4*^{Δ/Δ} HSC/HPC cultures (Fig EV2B). These data indicate that *Brd4* loss causes cell cycle arrest in HSC/HPCs.

Cell cycle arrest is one of the common features of senescent cells (Gorgoulis *et al*, 2019). Since senescence-associated beta-galactosidase (SA-beta-gal) (defined as beta-galactosidase activity) is the most widely used biomarker for detecting senescence in cells, we next performed β-galactosidase (β-Gal) staining on WT and *Brd4*^{Δ/Δ} LK cells to assess if loss of *Brd4* impacts on β-gal activity. Strikingly, there was a profound increase in the frequency of β-gal⁺ cells in *Brd4*^{Δ/Δ} LK cells compared to WT LK cells (Figs 3F and EV2C). To quantitatively measure senescence-associated β-gal activity in living cells, we next performed flow cytometry analysis using

Figure 2. Loss of *Brd4* results in the accumulation of hematopoietic stem cells and progenitor cells in BM.

- A Flow cytometric analysis of Lin[−], LT-HSC (long-term HSC), ST-HSC (short-term HSC), MPP (Multipotent progenitor), CMP (common myeloid progenitor), GMP (granulocyte/macrophage progenitor), and MEP (megakaryocyte-erythrocyte progenitor) cell populations in BM of representative WT, *Brd4*^{Δ/+}, and *Brd4*^{Δ/Δ} mice.
- B, C Quantitation of the percentage of HSC/HPC subpopulations in WT, *Brd4*^{Δ/+}, and *Brd4*^{Δ/Δ} mice (*n* = 6 per genotype). Lin[−], WT vs. *Brd4*^{Δ/Δ}, *P* < 0.0001; LKS[−], WT vs. *Brd4*^{Δ/Δ}, *P* < 0.0001; CMP, WT vs. *Brd4*^{Δ/Δ}, *P* < 0.0001; GMP, WT vs. *Brd4*^{Δ/Δ}, *P* = 0.0115; MEP, WT vs. *Brd4*^{Δ/Δ}, *P* = 0.0102; LSK, WT vs. *Brd4*^{Δ/Δ}, *P* = 0.0054; LT-HSC, WT vs. *Brd4*^{Δ/Δ}, *P* = 0.1153; ST-HSC, WT vs. *Brd4*^{Δ/Δ}, *P* = 0.0013; MPP, WT vs. *Brd4*^{Δ/Δ}, *P* = 0.2682. Comparisons among the groups were formed by one-way ANOVA.
- D CFU-C assay using 12,500 BMMNC cells from WT and *Brd4*^{Δ/Δ} mice. Biological replicates, *n* = 3, Group 50–500: *P* = 0.0619, Group > 500: *P* < 0.0001.
- E CFU-C assay using 100 LT-HSC cells from WT and *Brd4*^{Δ/Δ} mice, *n* = 6, biological replicates, *P* < 0.001.
- F Serial cell replating assays using BMMNC cells (3 mice per genotype, biological replicates). A total of 12,500 bone marrow mononuclear cells were used for each methylcellulose culture. The cells were replated weekly for 3 weeks.

Data information: Data are shown as the Mean ± S.E.M. Unpaired Student's *t*-test; **P* < 0.05 ***P* < 0.01, ****P* < 0.001. Source data are available online for this figure.

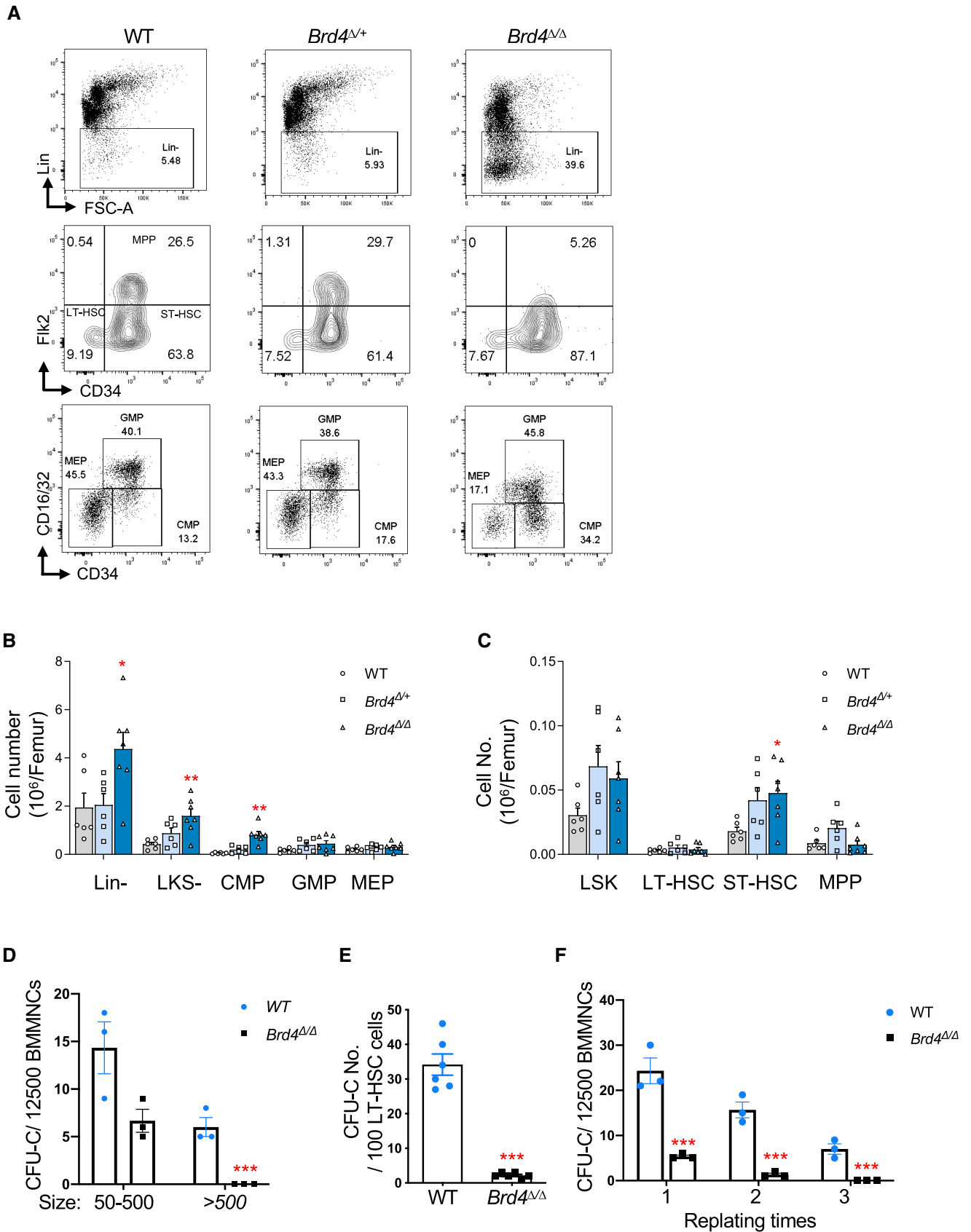


Figure 2.

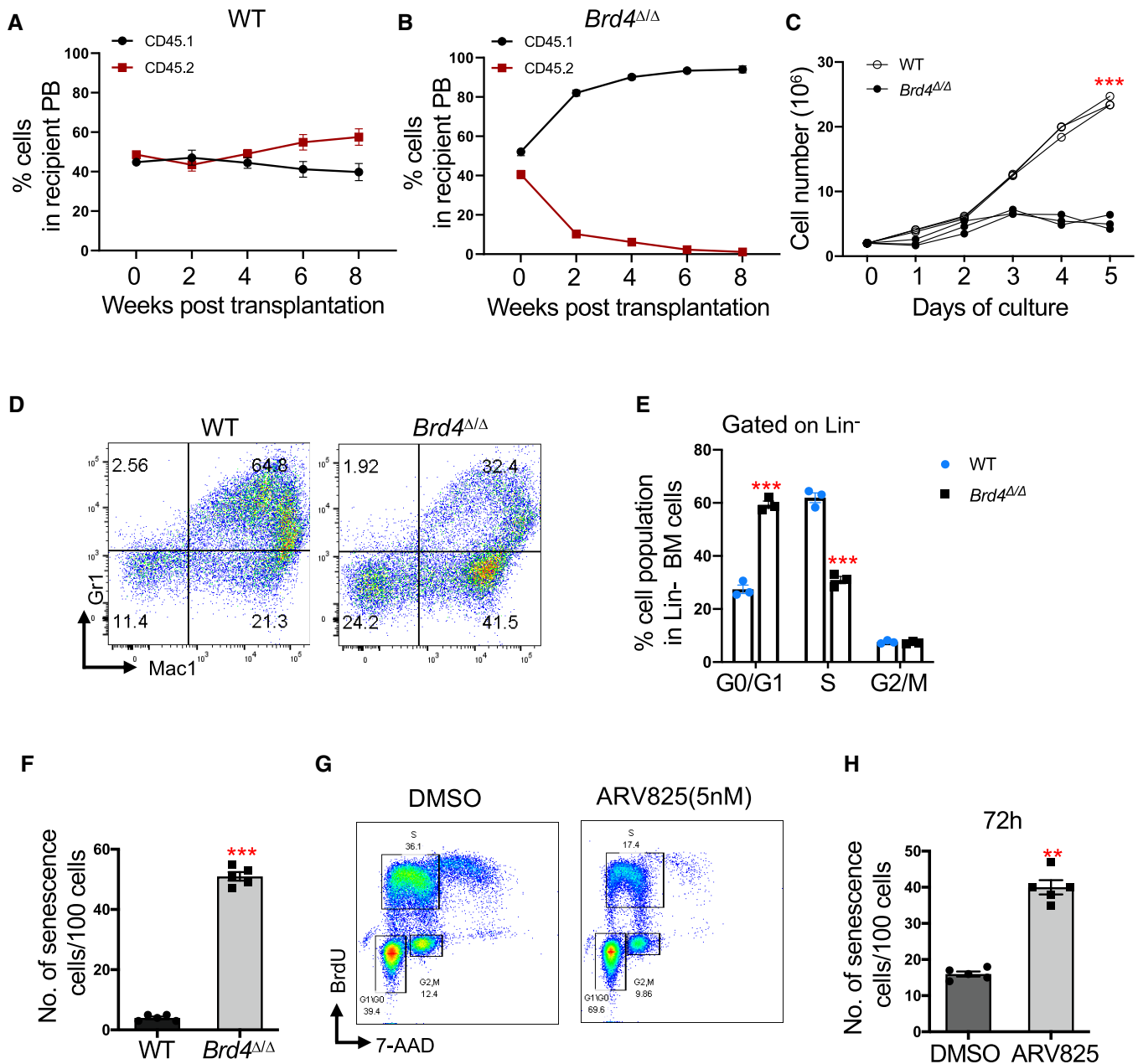


Figure 3. Loss of *Brd4* alters hematopoietic stem cell function.

A, B The percentages of donor-derived WT ($n = 5$, biological replicates) (A) or $Brd4^{\Delta/\Delta}$ ($n = 8$, biological replicates) (B) CD45.2⁺ cells versus CD45.1⁺ cells in the peripheral blood of recipient animals at indicated time points are shown.

C Cell number counting for the liquid culture of LK cells from WT and $Brd4^{\Delta/\Delta}$ mice. Biological replicates, $n = 3$, $P < 0.0001$.

D Flow cytometric analysis of myeloid cells in LK from WT and $Brd4^{\Delta/\Delta}$ mice 7 days after liquid culture.

E Quantitation of the cell cycle in WT and $Brd4^{\Delta/\Delta}$ mice. Biological duplicates, $n = 3$, G0/G1, $P = 0.0001$; S, $P = 0.00017$.

F Quantitation of the number of senescence cells per 100 LK cells from WT and $Brd4^{\Delta/\Delta}$ mice. Biological replicates, $n = 5$, $P < 0.0001$.

G Flow cytometric analysis of cell cycle for 32D cells with or without ARV825 treatment.

H Quantitation of the number of senescence cells per 100 32D cells after 72 h of ARV825 (5 nM) treatment, biological replicates, $n = 5$, $P < 0.0001$.

Data information: Data are shown as the Mean \pm S.E.M. Unpaired Student's t -test; * $P < 0.05$, ** $P < 0.01$, *** $P < 0.001$.

Source data are available online for this figure.

various cell populations. Compared to WT cells, all $Brd4^{\Delta/\Delta}$ cell populations had increased SA- β -gal activity (Fig EV2D). qPCR also revealed increased expression of senescence marker *Cdkn1a*,

Cdkn2a, and decreased expression of *Lamin B1* in $Brd4^{\Delta/\Delta}$ HSPCs, further supporting a role of BRD4 in senescence in hematopoietic stem/progenitor cells (Fig EV2E). To confirm the impact of *Brd4* loss

on cell cycle and senescence, we treated 32D cells, a mouse myeloblast-like cell line, with a BRD4-PROTAC degrader (ARV825). Consistently, 3 days of treatment with ARV825 led to an accumulation of cells in the G0/G1 population, and decreased cells in S-phase (Fig 3G), along with an increased frequency of β -Gal⁺ cells (Figs 3H and EV2F). Surprisingly, ARV825 had limited impact on the apoptosis in 32D cells (Fig EV2G), which is consistent with a minimal change in apoptosis in *Brd4*^{Δ/Δ} HSC/HPCs. To further confirm the role of BRD4 in senescence, ARV-825 were removed from the medium after 72 h treatment, and the cells were continued to be cultured for additional 7 days. The result showed an increased frequency of β -Gal⁺ cells accompanied by increased mRNA levels of *Cdkn1a* and *Cdkn2a*, two senescence markers, in ARV-825 pretreated 32D cells (Fig EV2H and I). However, the percentage of the apoptotic cells had minimal change in ARV825 treated cells (Fig EV2J). Collectively, these results demonstrate a suppressive role of BRD4 in HSC/HPC senescence.

Brd4 deletion alters transcriptional programs in HSC/HPCs

To investigate the impact of *Brd4* loss on transcriptome of HSC/HPCs, we performed RNA-seq on WT and *Brd4*^{Δ/Δ} LSK cells. We identified a total of 2,828 differentially expressed genes (DEGs), with 938 up-regulated and 1,890 down-regulated genes in *Brd4*^{Δ/Δ} LSK cells compared to WT LSK cells (Appendix Fig S2A, Appendix Table S1). Among those DEGs, several up-regulated DEGs are associated with myeloid differentiation and senescence, such as *Meis1*, *S100a8*, and *S100a9* (Appendix Fig S2B). We also observed reduced expression of *Vwf*, *Fcgr2b*, *Gata1*, *Aqp1*, *Ermap*, and *Klf1*, which are important for erythroid cell lineage commitment (Appendix Fig S2B). Gene set enrichment analysis (GSEA) revealed that *Brd4*^{Δ/Δ} HSC/HPCs had positive enrichment for genes associated with senescence (Fig EV3A and Appendix Fig S2C) and negative enrichment for genes associated with leukocyte proliferation (Fig EV3A). RNA-seq analysis of LK cells also showed increased expression levels of myeloid (*Meis1*) and senescence genes (*S100a8*, *S100a9*), and decreased expression of erythroid cell lineage genes (*Gata1*, *Klf1*) (Fig 4A and Appendix Fig S2D). A positive enrichment of genes associated with senescence was also prominent in *Brd4*^{Δ/Δ} LK cells (Fig 4B). Further analysis of SASP genes based on the gene list provided by two independent groups (Midha et al., 2021; Saul et al., 2022) revealed that the SASP gene sets are upregulated in *Brd4*^{Δ/Δ} LK cells as compared to WT cells (Fig EV3B and C, and Appendix Fig S2E and F).

Given HSC/HPC heterogeneity, we then performed single-cell RNA-seq (scRNA) of ~8,000 LSK and ~25,000 cKit⁺ cells from the BM of WT and *Brd4*^{Δ/Δ} mice to determine the transcriptional changes in different HSC/HPC populations upon *Brd4* loss. Twelve major clusters were identified by the unsupervised clustering method after integrating WT and *Brd4*^{Δ/Δ} cKit⁺ cells (Fig 4C), while four clusters were identified in LSK populations (Appendix Fig S2G). *Meis1*, *S100a8*, and *S100a9* were increased in all of the four clusters in *Brd4*^{Δ/Δ} compared with WT LSK cells (Appendix Fig S2H), consistent with the bulk RNA-seq result. Loss of *Brd4* altered the cluster distribution of cKit⁺ cells with a reduction in multiple subpopulations, including HSC (4.4 vs. 2.1%), MEP (9.6 vs. 3.4%), MKP (megakaryocyte progenitors) (4.8 vs. 1.7%), and EP (erythroid progenitor) (10.7 vs. 0.81%) (Appendix Fig S2I). In contrast, the preNeu (pre-neutrophil, late committed) and immNeu (immature neutrophil) clusters were drastically increased (14.9 vs. 37.3% and 0.02 vs. 3.8%, respectively) (Appendix Fig S2I). Analysis of the expression levels of subpopulation-specific gene signatures revealed a lower stemness score in *Brd4*^{Δ/Δ} compared to WT HSC/HPCs, despite a higher absolute number of HSC/HPCs in *Brd4*^{Δ/Δ} than WT mice (Fig 4D). Importantly, higher myeloid scores were identified in all of the *Brd4*^{Δ/Δ} HSC/HPC subpopulations (Fig 4E).

GSEA analysis revealed that loss of *Brd4* increased the expression of senescence-associated genes in all subpopulations of the HSC/HPCs (Fig 4F). Detailed analysis of computed signature scores confirmed the increased expression of senescence signature genes in multiple subpopulations of *Brd4*^{Δ/Δ} HSC/HPCs compared to WT, including HSC, MPP2, MPP3, CMP, proNeu, MEP, and MonoP (monocyte progenitors) (Fig 4G and Appendix Fig S2J and K). In contrast, the HSC signature genes were downregulated in *Brd4*^{Δ/Δ} HSC/HPCs compared to WT HSC/HPCs (Fig 4H). Additionally, *Brd4*^{Δ/Δ} HSC/HPCs had decreased expression of genes controlling cell cycle transition compared to WT cells. These data reinforce the importance of BRD4 in the maintenance of normal transcriptomic profiles in HSC/HPCs.

Brd4 loss alters chromatin accessibility in adult HSC/HPCs

Given the transcriptome alteration in *Brd4*^{Δ/Δ} versus WT HSC/HPCs, we wondered if *Brd4* loss changes chromatin accessibility. We, therefore, performed ATAC-seq using WT and *Brd4*^{Δ/Δ} LK cells (Appendix Fig S3A). There is a substantial increase in the average signal of accessible peaks in *Brd4*^{Δ/Δ} HSC/HPCs compared to WT HSC/HPCs (Fig 5A and Appendix Fig S3B), although the number of peaks was less in *Brd4*^{Δ/Δ} cells than WT cells (156,552 vs. 125,417

Figure 4. Loss of *Brd4* alters transcriptional lineage commitment in HSCs and progenitor cells.

- Heatmap of RNA-seq analysis shows the up- and downregulated genes in *Brd4*^{Δ/Δ} versus WT LK cells (FDR < 0.05 and fold change in log > 1).
- Gene set enrichment analysis (GSEA) shows that genes involved in the regulation of senescence are upregulated in *Brd4*^{Δ/Δ} LK cells. The normalized enrichment score (NES) and FDR are shown.
- Uniform manifold approximation and projection (UMAP) visualization of HSC/HPC clusters identified from WT and *Brd4*^{Δ/Δ} cKit⁺ cells. Each dot represents one cell, and cluster identity is color coded (Seurat). Left: Overlap of WT and *Brd4*^{Δ/Δ}. Right: the cluster representative of the UMAP visualization.
- Violin plot of stemness transcription signature in different subpopulations, Mann–Whitney *U*-test.
- Violin plot of myeloid transcription signature in different subpopulations, Mann–Whitney *U*-test.
- GSEA for gene sets of senescence in HSPC population in *Brd4*^{Δ/Δ} cells versus WT cells. The colors reflect scaled NES, representing the degree of expression change. The size of the circle represents the FDR value.
- UMAP visualization of HSC/HPC clusters identified from WT and *Brd4*^{Δ/Δ} cKit⁺ cells, colored by the signature score values of senescence gene sets.
- GSEA for gene sets of HSC and cell cycle in the HSPC population in *Brd4*^{Δ/Δ} cells versus WT cells. The colors reflect scaled NES, representing the degree of expression change. The size of the circle depicts the FDR value.

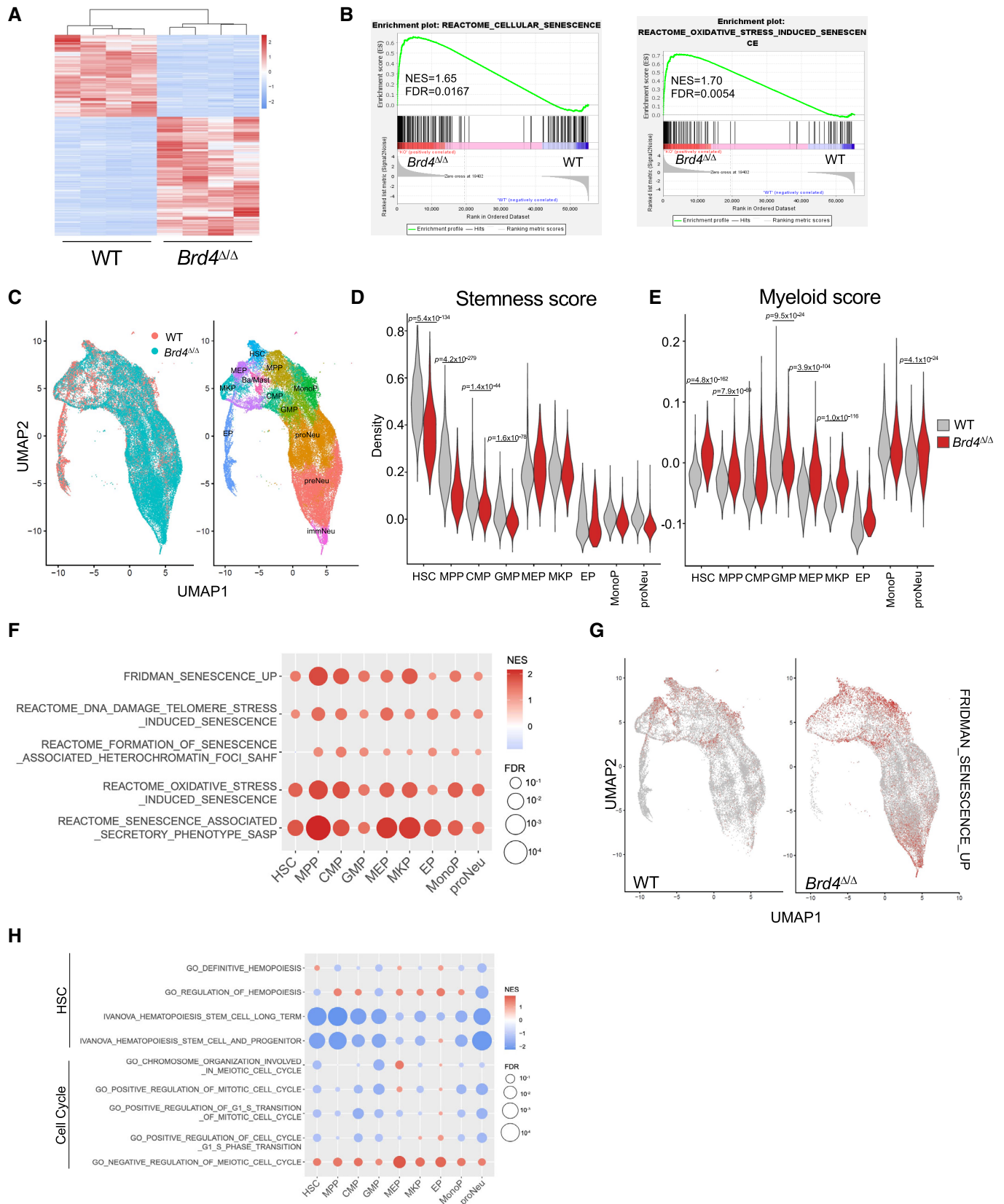


Figure 4.

peaks in WT vs. *Brd4*^{Δ/Δ} LK cells, respectively). The genome-wide distribution of the accessible peaks was similar between WT and *Brd4*^{Δ/Δ} cells (Appendix Fig S3C). Detailed analysis of the ATAC-seq data revealed that deletion of *Brd4* led to a reduction in 43,402 peaks and an increase in 22,426 peaks (Fig 5B). Enrichment analyses showed that the accessibility-increased peaks were enriched

for genes implicated in cellular senescence and myeloid cell development (Fig 5C). In contrast, the peaks with reduced accessibility were enriched for genes associated with regulation of cell cycle and cell growth (Fig 5D).

To uncover potential transcription factor (TF) networks that are potentially different between WT and *Brd4*^{Δ/Δ} LK cells, we next

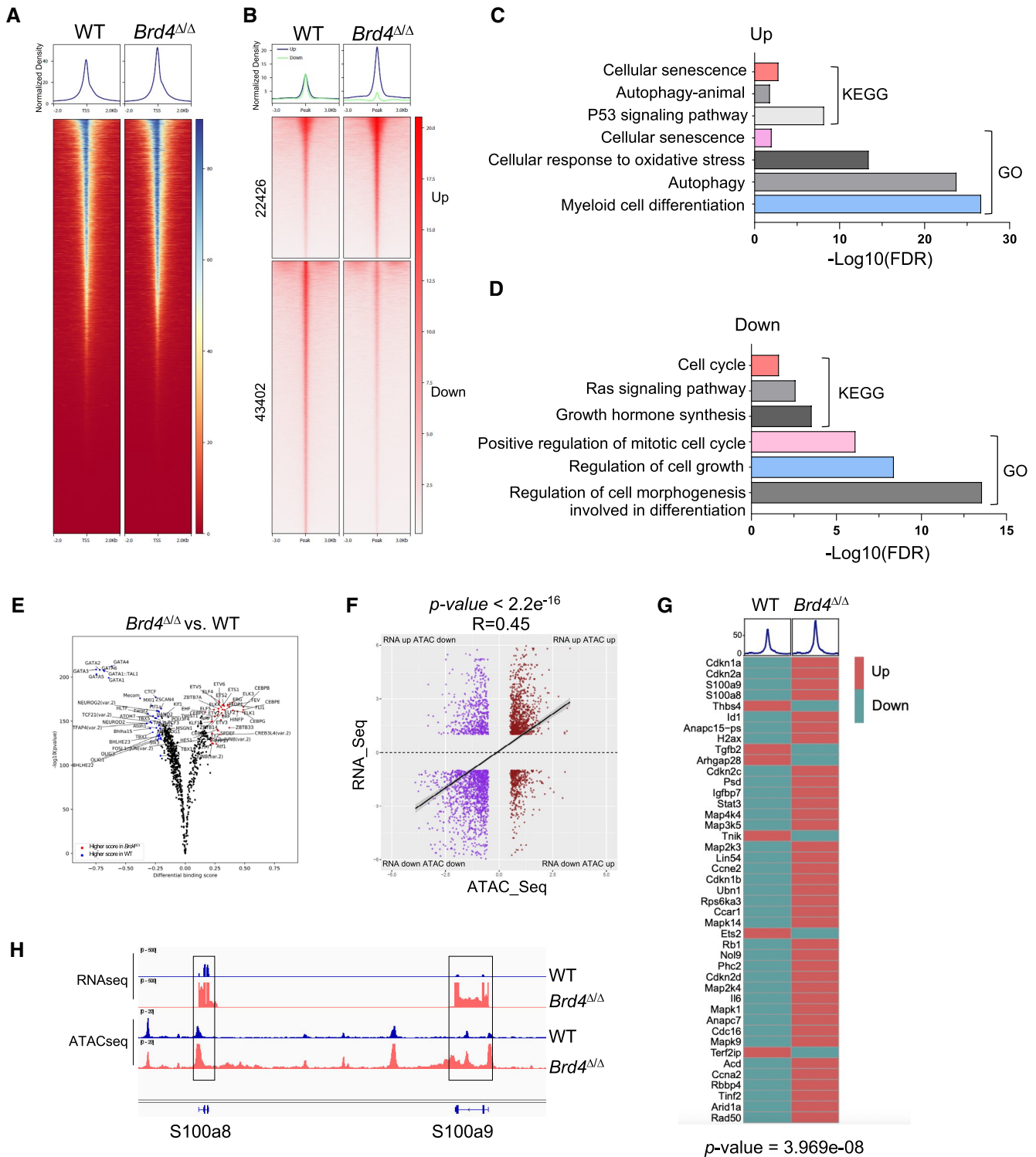


Figure 5.

Figure 5. Loss of *Brd4* altered chromatin accessibility and TF occupancy.

- A Heatmap of genome-wide ATAC-seq signal profile around TSS ($\pm 2,000$ bp).
- B Heatmap of accessibility signal profile among increased and decreased peak regions.
- C Functional enrichment analysis of genes with increased ATAC-seq peaks in *Brd4*^{Δ/Δ} compared with WT LK cells.
- D Functional enrichment analysis of genes with decreased ATAC-seq peaks in *Brd4*^{Δ/Δ} compared with WT LK cells.
- E Footprinting analysis with TOBIAS illustrates global changes in transcription factor footprint depth in *Brd4*^{Δ/Δ} versus WT LK cells. Each dot represents one transcription factor (TF). WT higher TFs are labeled as blue, and *Brd4*^{Δ/Δ} higher TFs are labeled as red.
- F The intersection of RNA-seq and ATAC-seq in LK cells. Promoter peak log₂FoldChange scores from ATAC-seq analysis (FDR < 0.05) and log₂FoldChange scores from RNA-seq analysis (DEGs) were tabulated and gene matched. Pearson's product-moment correlation test, *P*-value < 2.2e-16, *R* coefficient score = 0.45.
- G Heatmap displays the densities of ATAC-seq peaks on 42 senescence-activated genes (TSS ± 3 kb). *P*-value = 3.969e-08.
- H ATAC-seq tracks show chromatin accessibility at the S100a8 and S100a9 genes with RNA-seq reads coverage in WT and *Brd4*^{Δ/Δ} LK cells. Regions showing increased accessibility and increased gene expression in *Brd4*^{Δ/Δ} LK cells.

performed footprinting analysis (Bentsen *et al*, 2020) using the ATAC-seq datasets. We identified a massive gain in myeloid differentiation TF binding, such as CEBP family, FLI1, SPIC, and ERG in *Brd4*^{Δ/Δ} cells compared to WT cells (Fig 5E). We also observed a decrease in the binding sites of GATA family members, CTCF, and TWIST family members (Fig 5E). To determine the functional association of the differential ATAC-seq peaks, we performed integrated analyses for RNA-seq and ATAC-seq. When ATAC-seq promoter peaks were assigned to DEGs, we observed a positive correlation between chromatin accessibility and transcriptional output (Fig 5F). The ATAC-seq density revealed a substantial increase in chromatin accessibility in 42 senescence-related genes in *Brd4*^{Δ/Δ} compared to WT cells (Fig 5G and H). Therefore, the upregulation of senescence gene expression in *Brd4*^{Δ/Δ} HSC/HPCs may be associated with increased chromatin accessibility.

Increased H3K122ac and H3K4me3 enrichment underlies the activation of senescence-specific genes in *Brd4*^{Δ/Δ} HSC/HPCs

To determine how BRD4 regulates gene expression in HSC/HPCs, we performed CUT&RUN (cleavage under target and release using nuclease) assay to map BRD4 occupancy in WT LK cells, using *Brd4*^{Δ/Δ} LK cells as control. A total of 5,286 BRD4 peaks were identified (Fig 6A). These peaks were distributed widely over the genic and intergenic regions (Fig 6B), with ~60% of the peaks in promoter regions, ~16% in introns, and the rest (~16%) were in the intergenic

regions. To determine if BRD4 associates with DNA sequence-specific binding in HSC/HPCs, we performed *de novo* motif analysis for DNA sequences surrounding the BRD4-binding peaks. The motifs that passed the significance threshold resemble those bound by several known TFs. No unique *de novo* motif was identified for BRD4 binding (Fig 6C). Further analysis revealed that the BRD4-binding profile was positively correlated with highly expressed genes (Fig 6D), consistent with the role of BRD4 in gene regulation. Functional enrichment analyses for BRD4 peaks showed that BRD4 target genes were enriched in cellular senescence, cell cycle, and DNA repair (Fig 6E).

Since BRD4 is a reader of acetyl-lysine, we next performed CUT&RUN to compare the genome-wide distribution of several histone marks, including H3K27ac, H3K122ac, H3K4me3, H3K27me3, and H3K4me in *Brd4*^{Δ/Δ} vs. WT LK cells (Appendix Fig S4A). Integrative analysis for BRD4 binding and histone modification in WT cells showed that the genome-wide occupancies of BRD4 were highly correlated with H3K27ac (correlation score = 0.5298), H3K122ac (correlation score = 0.4383), and H3K4me3 (correlation score = 0.23; Fig 6F and G). In contrast, the genome-wide occupancies of BRD4 in WT cells were less correlated with H3K4me (correlation score = -0.2047) and H3K27me3 (correlation score = -0.0228; Fig 6F and G). Normalized global read density and locus-level enrichment revealed a significant genome-wide increase in H3K27ac, H3K122ac, and H3K4me3 occupancy in *Brd4*^{Δ/Δ} compared to WT LK cells (Fig 6H and Appendix Fig S4B). Convergent analysis

Figure 6. Genome-wide distribution of BRD4 in HSC/HPC cells.

- A BRD4 CUT&RUN signal in WT and *Brd4*^{Δ/Δ} HSC/HPCs.
- B Pie chart showing the distribution of BRD4-binding sites across genomic regions in HSC/HPCs.
- C *De novo* DNA sequence motifs identified in BRD4-bound regions.
- D Meta-gene tracks of BRD4 CUT&RUN signal averaged over all promoter-TSS tracks grouped by relative expression levels (highly expressed, TPM ≥ 1 ; lowly expressed, TPM < 1). X-axis, base pairs relative to TSS; Y-axis, BRD4 CUT&RUN signal intensity.
- E Enrichment analysis of genes with BRD4 bound in WT cells from KEGG and gene ontology database.
- F The signal correlation of BRD4 with other histone modifications from WT LK cells.
- G Correlation score of BRD4 with other histone modifications.
- H Global levels of histone modifications at peaks and flanking 3-kb regions. For each comparison, normalized coverages by sequencing depth were scaled to 100% and averaged in two biological replicates.
- I Scatter plots with linear fit show correlations between changes in H3K27ac, H3K122ac, and H3K4me3, and changes in gene expression in WT and *Brd4*^{Δ/Δ} LK cells. Pearson's correlation coefficient *R*-values are shown, *P*-value < 2.2e-16 for all correlation tests. X- and Y-axes show the log₂-transformed fold change (log₂FC) for each histone enrichment and mRNA expression level, respectively. DEGs are marked in red.
- J Boxplot of mean scores of histone modification CUT&RUN signals in 42 senescence-activated genes in WT and *Brd4*^{Δ/Δ} LK cells (TSS ± 5 kb). The bottom of the lower whisker, the bottom of the box, the middle band, the top of the box, and the top of the upper whisker represent the minimum, first quartile, median, third quartile, and maximum of histone modification levels on the 42 genes, respectively. The average of two biological replicates was used to quantify the level of specific histone modification level on each of the 42 senescence-associated genes.
- K Representative genome browser tracks showing H3K27ac, H3K122ac, H3K4me3, and H3K27me3 enrichment on the S100a8 gene.

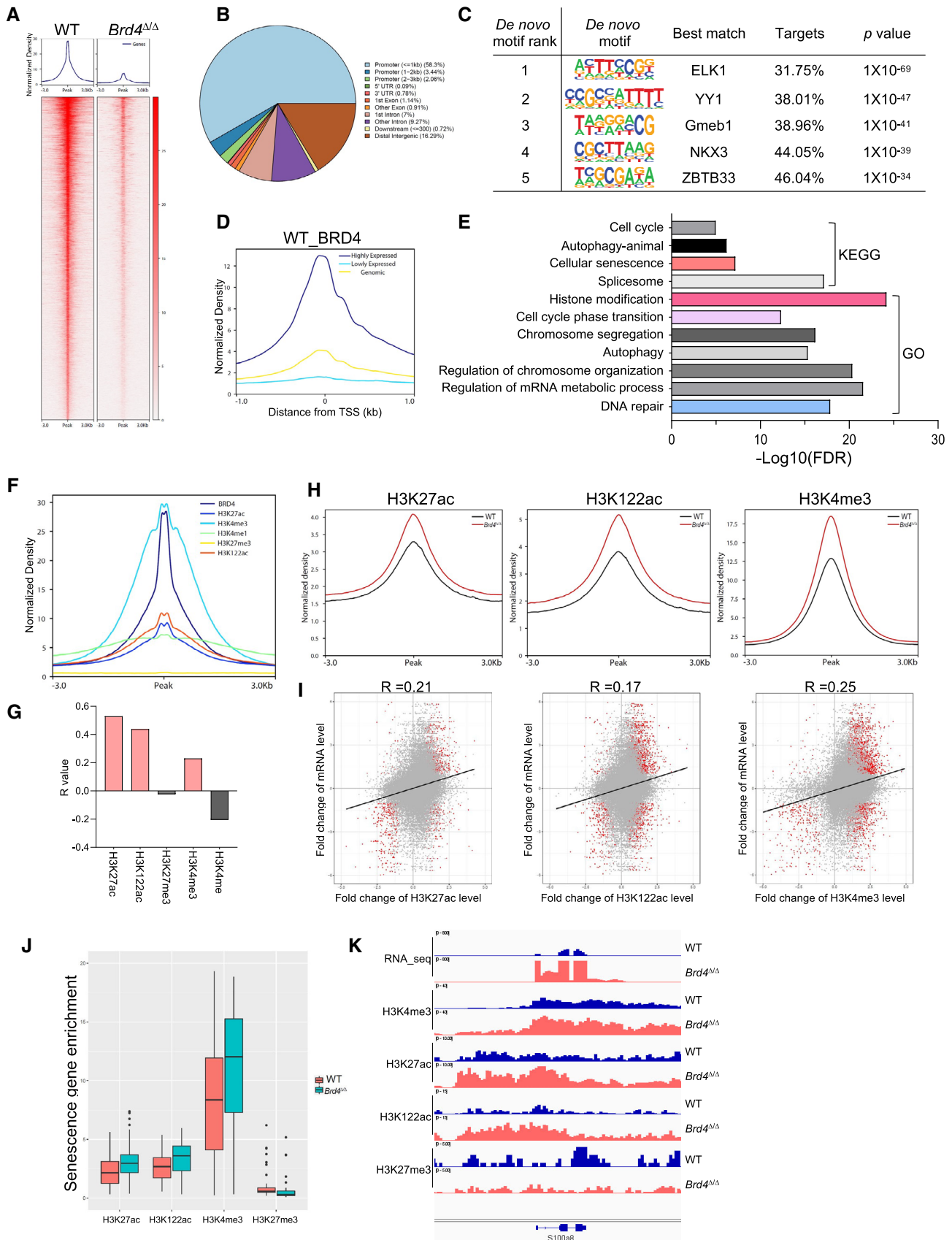


Figure 6.

of CUT&RUN and RNA-seq datasets showed that the DEGs were positively correlated with altered occupancies of the three histone marks, H3K27ac, H3K122ac, and H3K4me3 (Fig 6I). Compared to H3K27ac and H3K27me3, the genes with altered H3K122ac and H3K4me3 occupancies showed a greater degree of gene expression changes (Appendix Fig S4C). Specifically, *Brd4*^{Δ/Δ} LK cells had a substantial elevation in the occupancies of H3K27ac, H3K122ac, and H3K4me3 on most of the senescence-related DEGs (Fig 6J and K and Appendix Fig S4D). These data indicate a suppressive role of BRD4 in the senescence-specific genes in HSC/HPCs.

Loss of BRD4 induces histone H3 clipping in HSC/HPCs

To determine if loss of BRD4 affects global histone acetylation levels in HSC/HPCs, we performed Western blot analysis using different histone acetylation-specific antibodies. The acetylation levels for H3K14, H3K18, H3K27, and H3K122 were comparable in WT and *Brd4*^{Δ/Δ} LK cells (Fig 7A). However, we detected a faster migration of H3 in *Brd4*^{Δ/Δ} cells, which was partially acetylated at H3K27, H3K122, and H3K23 (Fig 7A). These smaller H3 proteins were recognized by H3 antibodies specific for the C-terminal but not N-terminal region, indicating the N-terminus cleavage. Because smaller H3 was not recognized by H3K14ac and H3K18ac antibodies, the cleavage site most likely lies at or within the K18-K23 or is not occurring within K14-K18 acetylated N-tails. When an H3 T22-cleaved specific antibody was used, a strong cleaved H3 band was detected in *Brd4*^{Δ/Δ}, but not WT LK cells (Fig 7A). Given the high specificity of the cleaved-H3 (T22) antibody (Cheung *et al*, 2021), it is most likely that the cleavage of H3 in *Brd4*^{Δ/Δ} cells occurred at the T22 site.

To identify which H3 isoform is proteolytically processed in *Brd4*^{Δ/Δ} progenitor cells, we conducted an *in vitro* H3 cleavage assay. WT or *Brd4*^{Δ/Δ} HSC/HPC cells (LK cells) were sorted by Lin⁻ and Ckit⁺ marker, the cell lysates were then incubated with full-length recombinant biotinylated H3.1, biotinylated H3.3, biotinylated H2A, and C-terminal His-tag H4, and the reaction products

were analyzed by immunoblotting with Streptavidin-HRP or HIS-HRP. The assay confirmed that the cleavage was observed in H3.3 but not in H3.1, H4, or H2A (Fig 7B, Appendix Fig S5A and B). Several proteases have been shown to have catalytic activities for histone H3 clipping, including cysteine protease Cathepsin L (CTSL1), Cathepsin G (CTSG), neutrophil elastase (ELANE), and proteinase 3 (PRTN3; Duncan *et al*, 2008; Cheung *et al*, 2021). ELANE and CTSG expression levels are elevated in *Brd4*^{Δ/Δ} LK cells, based on the RNA-seq data (Appendix Fig S5C). We next examined the impact of the proteases on H3 tail clipping by incubating full-length H3.3 with lysates of *Brd4*^{Δ/Δ} LK cells with or without CTSL, CTSG, and ELANE inhibitors. Addition of ELANEi (Fig 7C) and CTSLi (Appendix Fig S5D), but not CTSGi (Appendix Fig S5E), prevented the H3.3 clipping in *Brd4*^{Δ/Δ} LK cells, reinforcing the cleavage activity of both CTSL1 and ELANE for H3.

To investigate whether the clipped H3 (cH3) was incorporated into chromatin, we fractionated nuclear extracts of WT or *Brd4*^{Δ/Δ} LK cells into chromatin-free and chromatin fractions and blotted them with antibodies against cH3 and the C-terminal region of H3. cH3 products were detected only in the chromatin fraction of both WT and *Brd4*^{Δ/Δ} LK cells, and a much higher level of cleaved H3 was detected in *Brd4*^{Δ/Δ} chromatin fraction compared to that of WT cells (Fig 7D). To gain a better understanding of the role of cH3 on gene regulation, we performed CUT&RUN with cleaved H3 antibody (T22) on WT and *Brd4*^{Δ/Δ} LK cells (Appendix Fig S5F). There was a much higher number of cH3 peaks in *Brd4*^{Δ/Δ} LK cells (51,913) than WT cells (13,906). Only a small fraction of peaks (1,638) overlapped between the cH3 peaks in WT and *Brd4*^{Δ/Δ} LK cells (Appendix Fig S5G). In WT cells, approximately 18% of the cH3 peaks were found at promoter regions, ~16.7% at intron, and ~34% at the intergenic regions (Appendix Fig S5H). In contrast, a higher number of cH3 peaks (~30%) were found at the promoter regions in *Brd4*^{Δ/Δ} cells compared to WT cells (Appendix Fig S5H). The cH3 was highly enriched at the transcription start site (TSS) of highly expressed genes relative to the low-expressed genes and all genes within the whole genome in *Brd4*^{Δ/Δ} LK cells (Fig 7E). The cH3-occupied genes in *Brd4*^{Δ/Δ} LK cells were enriched

Figure 7. Loss of BRD4 induces histone 3.3 Clipping in HSC/HPC cells.

- Western blot analysis of WT and *Brd4*^{Δ/Δ} HSC/HPC nuclear protein with the indicated histone PTM-specific antibodies. Arrows indicate the cleavage product. The BRD4 level is also shown in Appendix Fig S1 using the same image.
- H3 cleavage assay of WT and *Brd4*^{Δ/Δ} HSPC cell lysate was analyzed by western blot with BRD4 and Streptavidin antibodies. Arrows indicated the cleavage H3.3.
- H3 cleavage assay of WT and *Brd4*^{Δ/Δ} HSPC cell lysate with or without ELANE inhibitor (ELANEi) were analyzed by western blot with BRD4 and Streptavidin antibodies. Arrows indicated the cleavage H3.3.
- WT and *Brd4*^{Δ/Δ} HSC/HPC cells were fractionated into chromatin-free (cytoplasmic and nuclear soluble) and chromatin fractions and blotted by indicated antibodies. Arrows indicate the cleavage H3.
- Association between cH3 enrichment and active transcription. The cH3 levels at the TSS-proximal regions of the genes grouped with relative expression level (highly expressed, TPM ≥ 1; lowly expressed, TPM < 1). X-axis, base pairs relative to TSS; Y-axis, cH3 CUT&RUN signal intensity.
- Enrichment analysis of genes with cH3 occupancy in *Brd4*^{Δ/Δ} HSC/HPC cells from KEGG and GO database.
- Venn diagram depicts the number of cH3 peaks-related genes identified in *Brd4*^{Δ/Δ} LK cells associated with accessible (ATAC-seq) peaks-related genes identified in *Brd4*^{Δ/Δ} LK cells.
- Venn diagram depicts the number of differential cH3 peaks-related genes identified between control and *Brd4*^{Δ/Δ} LK cells associated with BRD4-enriched peaks-related genes identified in control LK cells.
- Venn diagram depicts the number of differential cH3 peaks-related genes identified between control and *Brd4*^{Δ/Δ} LK cells associated with H3K122ac-enriched differential peaks-related genes identified between control and *Brd4*^{Δ/Δ} LK cells.
- Venn diagrams show the overlap among differential cH3_BRD4, cH3_H3K122ac, and cH3_H3K27ac peaks-related genes.
- Violin plot of mean scores within TSS ± 5 kb of cH3 CUT&RUN signals in 42 senescence-activated genes in WT and *Brd4*^{Δ/Δ} LK cells. Unpaired Student's t-test, P-value = 8.866e⁻¹⁰.
- ChIP-quantitative PCR for cH3 at senescence genes in BRD4 WT and *Brd4*^{Δ/Δ} HSC/HPC cells. Biological replicates: n = 3, Mean ± S.E.M; one-way ANOVA tests; P-values < 0.001 (cH3-*Brd4*^{Δ/Δ} vs. cH3-WT).

Source data are available online for this figure.

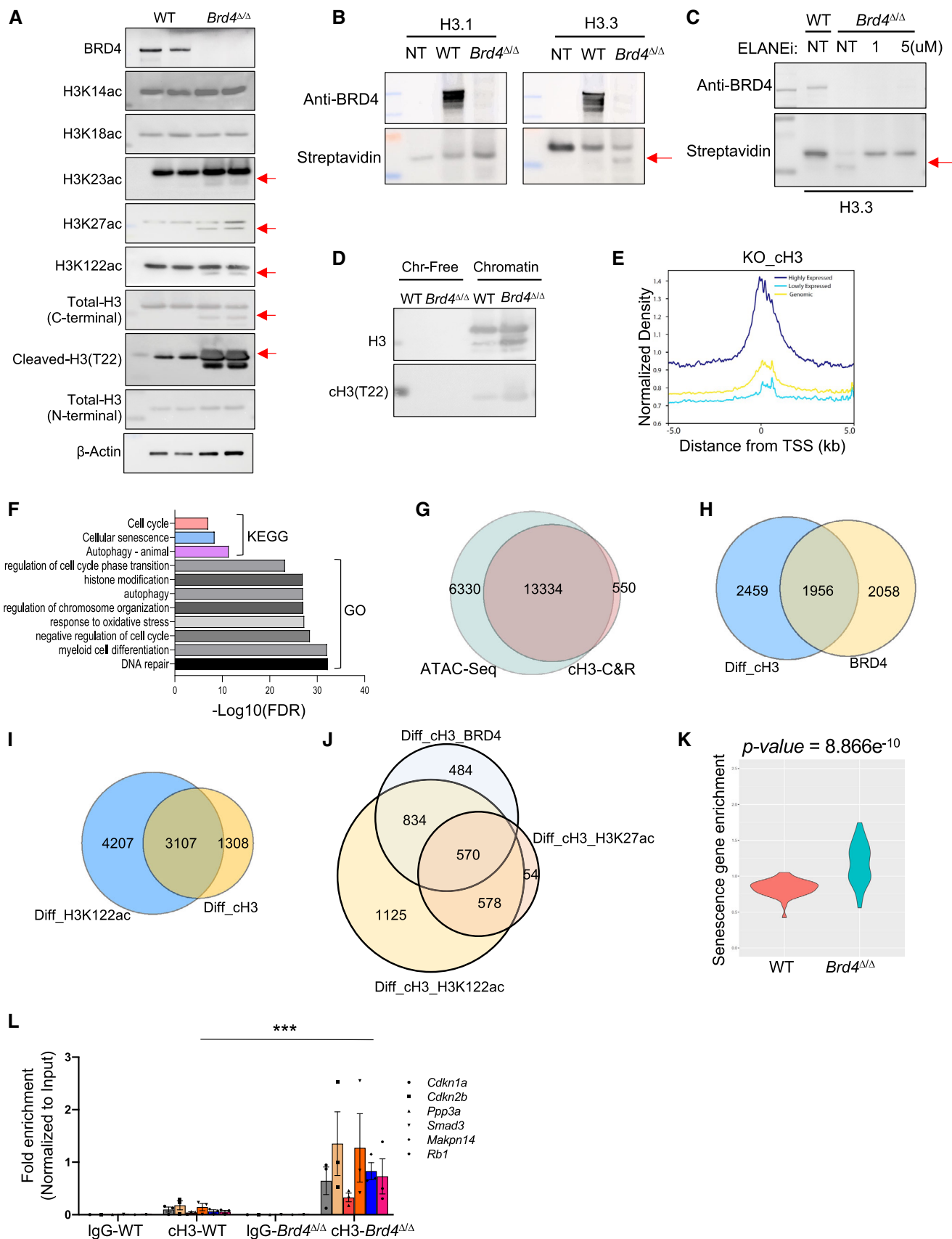


Figure 7.

for genes implicated in cellular senescence, cell cycle, myeloid differentiation, and DNA repair (Fig 7F).

To investigate the relationship between cH3 and chromatin accessibility, we performed convergent analysis with cH3 CUT&RUN and ATAC-seq datasets and found that 96% of the cH3 peaks-related genes overlapped with genes detected in ATAC-seq (Fig 7G). In addition, 49% of genes with BRD4 binding sites overlapped with *Brd4*^{Δ/Δ}-specific cH3-occupied genes (Fig 7H).

Brd4^{Δ/Δ}-specific cH3-occupied genes were highly overlapped with differential occupancies by H3K122ac (*Brd4*^{Δ/Δ} vs. WT, 70.3%) and H3K27ac (28.8%), but not with H3K27me3 (0.7%) (Figs 7I and EV3D and E). Further analysis revealed that the genes occupied by both BRD4 and cH3 were more likely to be modified by H3K122ac and H3K27ac (Fig 7J). Intriguingly, we observed significantly higher levels of cH3 peaks at the 42 senescence-related DEGs in *Brd4*^{Δ/Δ} compared to WT cells (Fig 7K). To further determine if SASP genes are regulated by cH3, we evaluated the occupancies of cH3 on SASP genes of WT and *Brd4*^{Δ/Δ} LK cells based on three different resources (REACTOME, Midha et al, 2021; Saul et al, 2022). There are significantly higher levels of cH3 occupancy at the SASP gene loci in *Brd4*^{Δ/Δ} cells compared to WT cells (Fig EV3F). These data reinforce an association between cH3 and SASP genes. ChIP-qPCR on selected senescence-related genes with cH3 and total H3 antibodies showed that the cH3 was highly enriched at the promoter regions of these genes in *Brd4*^{Δ/Δ} LK cells, but was hardly detected in WT cells, while the total H3 levels enriched in the promoter regions were similar between WT and *Brd4*^{Δ/Δ} LK cells (Fig 7L and Appendix Fig S5I).

To verify the functional consequences of ectopic expression of cH3.3 on HSC/HPCs, we transduced GFP-tagged H3.3 or cH3.3 into 32D cells and performed CFU-C and senescence assays. GFP⁺ 32D cells with cH3 ectopic expression had higher frequency of β-gal⁺ cells compared to H3.3-expressing 32D cells (Fig 8A and Appendix Fig S6A). Furthermore, overexpression of cH3 in 32D cells reduced the number and the size of CFU-Cs compared to H3.3 expression (Fig 8B and Appendix Fig S6B). To assess the impact of cH3.3 ectopic expression on the expression of SASP genes, we performed qPCR for *Cdkn1a* and *Cdkn2a* using the cells ectopic-expressing cH3.3. The data showed overexpression of cH3.3 increases the expression of *Cdkn1a* and *Cdkn2a* (Appendix Fig S6C). These studies verified a role of cH3 in senescence and colony-forming activity.

To further verify the role of BRD4 in senescence, we crossed *Brd4*^{fl/fl}; *Mx1Cre*⁺ mice with *Brd4* transgenic mice (*Brd4*^{OE}) (Appendix Fig S6D) and compared the cH3 level and β-gal⁺ cell frequency between *Brd4*^{Δ/Δ} and *Brd4*^{OE}; *Brd4*^{Δ/Δ} LK cells. Re-expression of BRD4 in *Brd4*^{Δ/Δ} LK cells reduced cH3 level to that of WT cells (Fig 8C) and significantly decreased the frequency of β-gal⁺ cells (Fig 8D and E). In contrast, the colony-forming capacity was significantly increased in *Brd4*^{OE}; *Brd4*^{Δ/Δ} BM cells compared with *Brd4*^{Δ/Δ} BM cells (Fig 8F). Collectively, these data demonstrate the essential role of BRD4 in maintaining normal HSC/HPC functions by suppressing H3 clipping-mediated cell senescence.

Discussion

HSCs have the ability to both retain their self-renewal and differentiation capacity into all hematopoietic lineages. The balance between self-renewal and differentiation is crucial for maintaining the HSC pool

and appropriate lineage distribution. *Brd4* is ubiquitously expressed throughout the differentiation hierarchy of HSCs, and overexpressed in AML (Bansal et al, 2017; Lee et al, 2018; Ozer et al, 2018; Lu et al, 2020). Here, we show that conditional deletion of *Brd4* in the adult hematopoietic system is lethal to mice. Deletion of *Brd4* in the adult hematopoietic system resulted in less mature erythroid cells and more immature myeloid cells in the BM of *Brd4*^{Δ/Δ} mice compared to WT mice. Surprisingly, loss of BRD4 led to a significant increase in HPCs (Lin⁻, LKS⁻, CMP, and GMP populations) among the BM cells compared to WT and *Brd4*^{Δ/+} mice. However, *Brd4*^{Δ/Δ} HSC/HPCs had limited colony-forming capacity and self-renewal activity as determined by both *in vitro* CFU-C replating assays and *in vivo* competitive transplantation assays. These data indicate that BRD4 is required for normal HSC/HPC function and that the *Brd4* loss-associated HSC/HPC dysfunction is cell autonomous. While BET inhibitors show promising effects in clinical trials in AML (Berthon et al, 2016), they also produce hematological side-effects, such as thrombocytopenia (Amorim et al, 2016). Our study indicates that BRD4 is essential for normal HSC/HPC behavior, reinforcing the necessity of close monitoring of blood counts during BETi treatment.

It has been shown that BRD4 interacts with P-TEFb, thereby stimulating its kinase activity in phosphorylating the carboxy-terminal domain of RNA pol II to promote target gene transcription (Itzen et al, 2014). Our RNA-seq and scRNA-seq results revealed that *Brd4* deficiency dysregulates the expression of genes key for the development of myeloid (*Meis1*) and erythroid (*Gata1*), as well as senescence (*S100a8* and *S100a9*). We also found that BRD4 loss increased chromatin accessibility along with a massive gain of the binding of TFs related to myeloid or HSC differentiation, such as CEBP family, FLI1, PU.1, and ERG, suggesting a positive correlation between chromatin accessibility and transcriptional output. Emerging evidence has linked the transcriptional consequences of BET inhibition to the association of BRD4 with enhancer elements, which could be involved in lineage-specific gene regulation (Loven et al, 2013; Roe et al, 2015; Lee et al, 2017). Our study showed that BRD4 is preferentially bound to the proximal (promoter), rather than the enhancer region in HSC/HPCs. BRD4 is known to have acetyltransferase activity and to evict nucleosomes through H3K122ac (Donati et al, 2018). Interestingly, we found an increased global occupancy of H3K27ac and H3K122ac, which is positively associated with gene expression. *Brd4* deletion mediated increased chromatin accessibility and increased occupancies of H3K27ac and H3K122ac of 40 senescence-related genes, which likely contributed to the defective *Brd4*^{Δ/Δ} HSC/HPC functions.

It has been suggested that histone tail clipping functions as an epigenetic regulatory mechanism in the differentiation of monocytes and embryo stem cells, and cellular senescence (Iwasaki et al, 2013; Cheung et al, 2021). Our ATAC-seq and cH3 CUT&RUN data provide direct evidence that H3 clipping was associated with chromatin accessibility and transcriptional activation. Fifty percent of BRD4-occupied genes were co-occupied by cH3 in *Brd4*^{Δ/Δ} HSC/HPCs, pointing to a role of BRD4 in protecting the histone from clipping. We further observed a concurrent cH3 with H3K122ac and H3K27ac modifications, but not H3K27me3 modification, in the *Brd4*-deleted cells, suggesting an important role of cH3 in epigenetic regulation. Further studies regarding the mechanisms under the crosstalk between histone modification and histone H3 clipping are warranted.

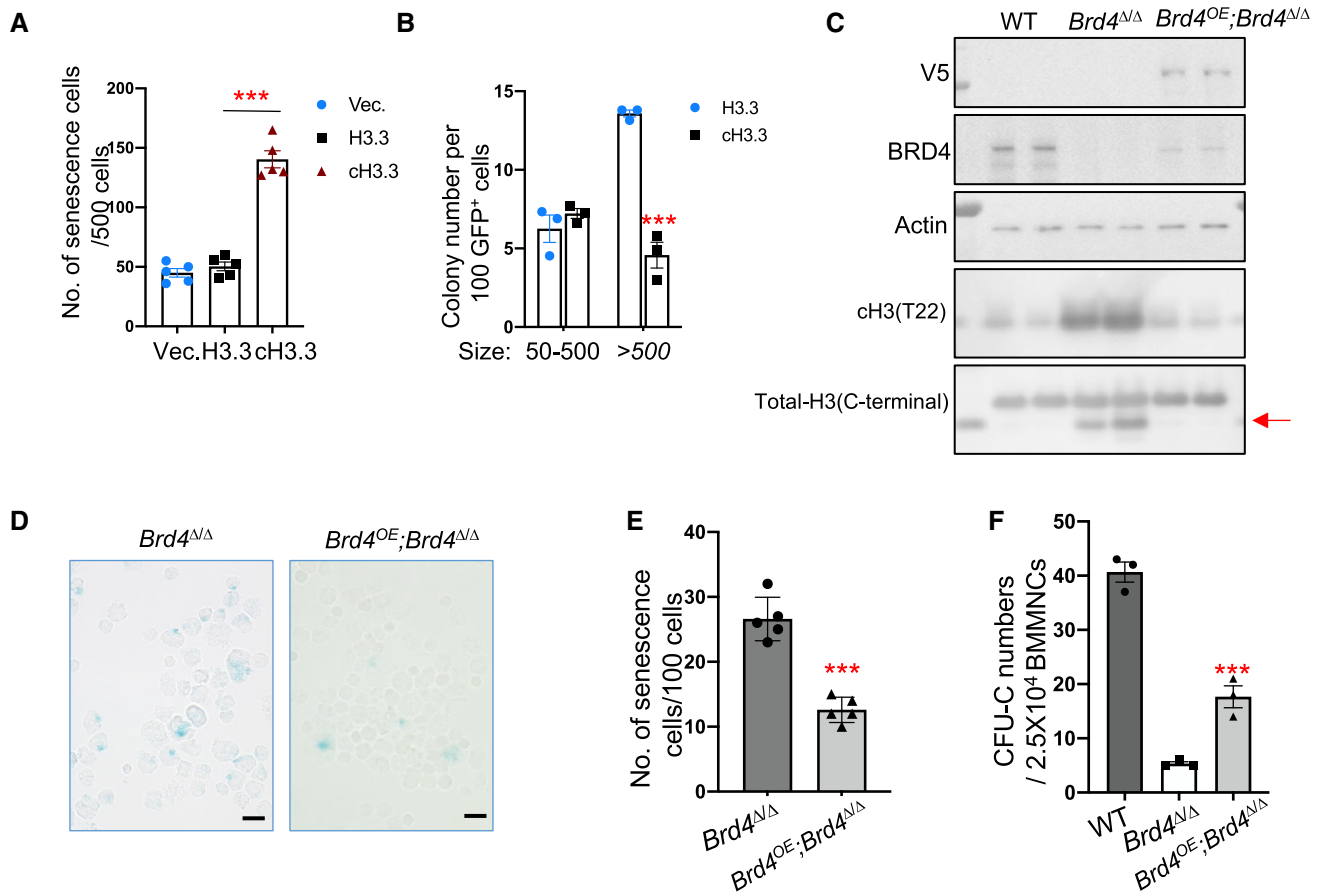


Figure 8. Re-expression of *Brd4* rescues the senescence phenotype.

- A Quantification of β -gal⁺ cells per 500 cells in 32D cells expressing the indicated histones; Mean \pm S.E.M. ($n = 5$ biological replicates); Unpaired Student's t -test; *** P -values < 0.001 (cH3.3 vs. H3.3).
- B Quantification of colony numbers per 100 GFP⁺ cells for colony formation assay with 32D cells expressing the indicated histones. Colony size > 500 cells, *** P -values = 0.0005; colony size from 50 to 500 cells, P -values = 0.35. Mean \pm S.E.M. ($n = 5$ biological replicates); unpaired Student's t -test.
- C Western blot analysis of nuclear protein from WT, *Brd4* $\Delta\Delta$, and *Brd4*^{OE}; *Brd4* $\Delta\Delta$ HSC/HPCs with the indicated antibodies. Arrows indicated the cH3 product.
- D Representative of senescence staining for gated LK cells from *Brd4* $\Delta\Delta$ and *Brd4*^{OE}; *Brd4* $\Delta\Delta$ mice, scale bar, 10 μ m.
- E Quantitation of the frequency of senescence cells per 100 LK cells from *Brd4* $\Delta\Delta$ and *Brd4*^{OE}; *Brd4* $\Delta\Delta$ mice. Biological replicates, $n = 5$, unpaired Student's t -test; *** P -values < 0.001 . Data are shown as the Mean \pm S.E.M.
- F CFU-C assay using 2.5×10^4 BMMNC cells from WT, *Brd4* $\Delta\Delta$ and *Brd4*^{OE}; *Brd4* $\Delta\Delta$ mice. Biological replicates, $n = 3$ unpaired Student's t -test; *** P -values < 0.001 . Data are shown as the Mean \pm S.E.M.

Our *in vitro* histone clipping assay confirmed that the clipping occurs on H3.3, but not H3.1. Surprisingly, we observed increased occupancies of both H3K4me3 and cH3 on the same gene sets in *Brd4* $\Delta\Delta$ HSC/HPCs. It is possible that H3K4me3 are on H3.1 but not H3.3. Another possibility is that H3K4me3 and cH3 are on different, but neighbor nucleosomes. Future study with ChIP-reChIP (using antibodies against cH3.3, H3.3, H3.1, and H3K4me3) is warranted to determine whether H3K4me3 and cH3 affect different gene pools.

CUT&RUN for cH3 and enrichment analysis implied the association of senescence with cH3. The ectopic expression of cH3.3 but not H3.3 is sufficient to induce the senescence phenotype and key gene expression. Duarte *et al* reported that overexpression of H3.3 can induce senescence. The different findings could be due to the different cell systems (hematopoietic stem/progenitor cells vs. fibroblasts).

Collectively, we identified a role of BRD4 in protecting chromatin integrity by preventing histone H3 clipping, especially at genomic

loci of senescence-related genes, thus maintaining normal HSC/HPC functions.

Materials and Methods

Mice

All animal experiments were done in accordance with the guidelines of the University of Texas Health San Antonio Animal Care and Use Facility.

Generation of *Brd4*-deficient mice

Brd4^{fl/fl} mouse is a kind gift from Dr. Nagi G. Ayad. *Brd4*^{fl/fl} mice were generated as previously described (Penas *et al*, 2019).

Brd4^{fl/fl} mice were crossed with *Mx1cre⁺* mice. *Brd4^{fl/fl}*, *Brd4^{fl/+}*, or *Brd4^{+/+}* mice were genotyped by PCR with primers p1 (Forward: 5'-TTTGACCTCTGCTCGTGTAGTG-3', Reverse: 5'-CATTGTACCCAGGCTCCTTTCA-3') using the following program: 95°C for 3 min, followed by 35 cycles of 95°C 15 s, 58°C 30s, and 72°C for 50s, and then 72°C for 5 min. The WT allele was detected at 485 bp, and the floxed allele was detected at 705 bp.

Generation of *Brd4* full-length transgenic mouse model (*Brd4^{OE}*)

The entire coding region of the mouse BRD4 isoform 3 (NM_001286630.1) was cloned into the HS321/45-vav vector. The plasmid DNA was digested with *SacII* to remove the pBSISK backbone and was used for injection into pronuclei of eggs from C57BL/6 mice (Cyagen US Inc). *Brd4^{OE}* transgenic mice were crossed with *Brd4^{fl/fl}* mice to obtain *Brd4^{OE}*, *Brd4^{Δ/Δ}* mice.

Phenotypic analyses of the hematologic system in mice

To induce *Brd4* deletion in the hematopoietic system, 6- to 8-week-old *Brd4^{fl/fl}*; *Mx1cre⁺* mice and *Brd4^{fl/fl}*; *Mx1cre⁻* mice were injected with polyinosinic:polycytidylic acid (*pl:pC*, 10 mg/kg) every other day for three injections. The deletion was confirmed by PCR for recombination band 1 week after the *pl:pC* injection. All mice were analyzed between 2 and 3 weeks after *pl:pC* injection. Peripheral blood (PB) was collected by retro-orbital bleeding and subjected to blood count (Hemavet System 950FS). May-Grünwald-Giemsa-stained PB smears, and cytopins of bone marrow and spleen cells were used for morphological analyses. Hematoxylin and eosin (H&E)-stained femur, spleen, and liver sections were used for histopathology analyses. Slides were visualized under a Keyence BZ-X810 fluorescence microscope. Images were taken by BZ-X800-Viewer software.

RNA extraction and RT-PCR

Total RNA was extracted using RNeasy Plus Mini Kit (Qiagen, Cat#74136) and subjected to RT-PCR and RNA-seq. Deletion of *Brd4* and the expression of *Brd4* at mRNA level in the subpopulation of HSPCs and different hematopoietic lineages were detected using real-time primer *mBrd4*-total (Forward: 5'-ACACCCATGGATATGGGAACAA-3', Reverse: 5'-CTTCTCCAGAGCTTCTGCCA-3'). GAPDH used as internal control (Forward: 5'-CGTCCGTAGACAAAATGGT-3', Reverse: 5'-TTGATGGCAACAATCTCCAC-3').

Western blot

Nuclear protein was extracted from *Lin⁻ Ckit⁺* cells. The following antibodies were used for western blot analysis: BRD4 (active motif, #39909), Histone H3 (C-terminal, Sigma, H0164), Histone H3 (N-terminal, Sigma H9289), H3K14ac (Millipore-Sigma, 07-353), H3K18ac (Millipore Sigma, 07-354), H3K23ac (Millipore-Sigma, 07-355), H3K27ac (Diagenode, C15410174), H3K122ac (Abcam, ab33309), Cleaved H3 (T22) (Cell Signaling Technology, 12576S), Anti-His (Abcam, ab18184), β -Actin (Cell signaling Technology, 3700S), anti-V5 (Millipore-Sigma, V8012), and Streptavidin-HRP (Abcam, ab7403).

Flow cytometry analysis and cell sorting

All mice for flow cytometry analysis and cell sorting were analyzed between 2 and 3 weeks after *pl:pC* injection. Total white blood cells were obtained after lysis of PB with red cell lysis buffer (Qiagen, Cat#158904). Single-cell suspensions of the cells from BM, spleen, liver, and PB were stained with panels of fluorochrome-conjugated antibodies (Appendix Table S3). The cell apoptosis analysis was performed on freshly isolated BM cells following staining with lineage/cKit antibodies and PE-Annexin V/7-AAD according to the protocol apoptotic kit (BD Biosciences, Cat#559763). Percentages of apoptotic cells in the *Lin⁻* subpopulation, and *Lin⁻cKit⁺* (LK) subpopulation were calculated. For cell cycle analysis, BM cells were labeled with BrdU for 45 min *in vitro* according to the instruction of FITC BrdU Flow Kit (BD Biosciences, Cat#559619), stained with surface markers, treated with DNase, and finally stained with FITC-conjugated anti-BrdU followed by 7-AAD staining. All flow cytometric analyses were performed using a BD FACS Canto II or LSR Fortessa flow cytometer. All data were analyzed using FlowJo_V10 software (Ashland, OR).

For HSC/HPC cell selection, BM cells were sorted with lineage depletion beads (Miltenyi Biotec, 130-110-470). The *Lin⁻* cells were then stained with the following panels of antibodies to sort subpopulation of HSC/HPC: LK cells (*Lin⁻*, *CD117⁺*), LSK (*Lin⁻*, *CD117⁺*, *Sca1⁺*), LT-HSC (*Lin⁻*, *CD117⁺*, *Sca1⁺*, *CD34⁻*, *FLK2⁻*), ST-HSC (*Lin⁻*, *CD117⁺*, *Sca1⁺*, *CD34⁺*, *FLK2⁻*), MPP (*Lin⁻*, *CD117⁺*, *Sca1⁺*, *CD34⁺*, *FLK2⁺*), CMP (*Lin⁻*, *CD117⁺*, *Sca1⁻*, *CD34⁺*, *CD16/32⁻*), MEP (*Lin⁻*, *CD117⁺*, *Sca1⁻*, *CD34⁻*, *CD16/32⁻*), and GMP (*Lin⁻*, *CD117⁺*, *Sca1⁻*, *CD34⁺*, *CD16/32⁺*). After 1 h of staining, the cells were washed with PBS and subjected to sorting with FACSAria (BD) cell sorter. For lineage cell sorting, the bone marrow mononuclear cells were stained with different panels of antibodies for subpopulations of cells, including neutrophils (*Mac1⁺Gr1⁺*), monocytes (*Mac1⁺Gr1⁻*), megakaryocytes (*CD41⁺CD61⁺*), erythroid cells (*Ter119⁺*), *CD4⁺* T cells (*CD3⁺CD4⁺*), *CD8⁺* T cells (*CD3⁺CD8⁺*), and B cells (*B220⁺*).

Cell senescence assay

Cell senescence analyses of bone marrow or 32D (ATCC CRL-11346) cells were performed on cytopins followed by staining using senescence cells histochemical staining kit (Sigma-Aldrich, Cat#CS0030-1KT). Slides were visualized under a Keyence BZ-X810 fluorescence microscope. Images were taken using BZ-X800-Viewer software. For senescence analysis using flow cytometry, BM cells were labeled with cell surface antigens with antibodies. Then, the cells were washed in 1% BSA in PBS and resuspended in 100 μ l fixation solution (4% paraformaldehyde in PBS). After 10 min of incubation, the cells were washed in 1% BSA in PBS and then resuspended in 100 μ l of working solution (1:500 dilution of CellEvent Senescence Green Probe into CellEvent Senescence buffer) according to the instruction of the Senescence Green Flow Cytometry Assay Kit (Thermo Fisher, Cat#C10841). The cells were incubated for 1–2 h at 37°C without CO₂. All of the data were analyzed using FlowJo-V10 software.

Colony-forming unit (CFU) cell assay

For CFU-C assays, total bone marrow or LT-HSC cells were plated in triplicate in methylcellulose medium (Methocult M3134, StemCell

Technologies, 03134) supplemented with mouse stem cell factor (mSCF, 100 ng/ml), human interleukin 6 (hIL-6, 50 ng/ml), interleukin 3 (mIL-3, 5 ng/ml), erythropoietin (EPO, 4 U/ml), thrombopoietin (mTPO, 100 ng/ml), and granulocyte–macrophage colony-stimulating factor (mGM-CSF, 10 ng/ml). The frequencies of CFU-Cs were scored on day 7 of the cultures.

For CFU-C assays using 32D cells, 1,000 cells were plated in triplicate in methylcellulose medium (Methocult M3134, StemCell Technologies, 03134) supplemented with interleukin 3 (mIL-3, 5 ng/ml) and 10% FBS. The pictures of the CFU-C were visualized under a Keyence BZ-X810 fluorescence microscope. Images were taken using BZ-X800-Viewer software.

High-proliferating potential colony-forming cells (HPP-CFCs) assay

To determine the growth of HPP-CFCs, bone marrow mononuclear cells (1×10^5) from WT, *Brd4*^{Δ/Δ} mice were cultured in triplicate in six-well plates with soft agar supplemented with mSCF (100 ng/ml), human IL-6 (50 ng/ml), hFlt3L (10 ng/ml), mIL-3 (10 ng/ml), mGM-CSF (10 ng/ml), and mG-CSF (10 ng/ml). Cultures were incubated at 5% CO₂, 5% O₂, and scored by indirect microscopy on day 14 for scoring the frequencies of HPP-CFCs in the cultures.

Competitive transplantation assays

The competitive repopulation assays were performed as previously described (Yang et al, 2018). Briefly, the transplantation was performed by tail vein injecting 1×10^6 BM cells from WT and *Brd4*^{Δ/Δ} mice (CD45.2⁺) along with 1×10^6 competitor BM cells from B6.SJL mice (CD45.1⁺) into lethally irradiated (950 cGy) recipients (CD45.1⁺) by tail vein injection.

In vitro liquid culture assay

Purified LK cells were plated into six-well plates containing RPMI-1640 medium, 10% fetal bovine serum (FBS), 1% penicillin–streptomycin, mSCF (100 ng/ml), hEPO (4 U/ml), hTPO (100 ng/ml), mIL-3 (5 ng/ml), and mGM-CSF (10 ng/ml). The cells were then collected for flow cytometric analysis and cytopins.

Drug treatment

BRD4 degrader ARV825 were bought from selleckchem (S8297). CTSL inhibitor is bought from Sigma (219421). CTSGi (Cathepsin G inhibitor) is bought from Sigma (219372). ELANEi (GW311616) is bought from MedChemExpress (HY-15891). For drug treatment, 32D cells were treated with 5 nM ARV-825 for 72 h. LK cells sorted from the BM of WT and *Brd4*^{Δ/Δ} were lysed in histone clipping buffer with CTSLi (10 μM), CTSGi (1 μM, 5 μM), and ELANEi (1 μM, 5 μM) for 3 h. DMSO was used as non-treatment (NT) control.

In vitro histone clipping assay

LK cells purified from the BM of WT and *Brd4*^{Δ/Δ} were lysed in buffer (10 mM HEPES, 10 mM KCL, 1.5 mM MgCl₂, 0.34 M sucrose, 10% glycerol, and 5 mM beta-mercaptoethanol). The lysate was then incubated with 500 ng biotinylated H3.3 (Active motif, 31297),

biotinylated H3.1 (Active motif, 31296), biotinylated H2A (Amsbio, 52049) and c-terminally 6xHis-tag H4 (Active motif, 31493) at 37°C for 1–3 h, and subjected to western blot analysis.

Chromatin fractionation

Purified LK cells (1×10^6) from WT and *Brd4*^{Δ/Δ} mice were resuspended in buffer I (10 mM HEPES-KOH, 1.5 mM MgCl₂, 10 mM KCl, 10% glycerol, 0.1% triton-X, supplemented with protease inhibitor cocktail, and 1 mM DTT) and incubated on ice for 10 min. Nuclei were harvested by 850 g centrifuge for 10 min at 4°C followed by twice washing with buffer I. The pelleted nuclei were then resuspended in the buffer II (10 mM HEPES-KOH, 1.5 mM MgCl₂, 10 mM KCl, 500 mM NaCl, 10% glycerol, 0.1% triton-X, supplemented with protease inhibitor cocktail, and 1 mM DTT). The chromatin fraction was recovered by centrifugation at 950 g for 5 min. The supernatant from this step is chromatin-free fraction. The chromatin fraction was then resuspended by buffer II, and benzonase was added for DNA digestion at RT for 30 min. After centrifugation at 7,000 g for 10 min, the supernatant from this step is chromatin fraction. The chromatin-free fraction and chromatin fraction were then used for western blot.

Plasmid construction and lentiviral transduction

Mouse full-length histone 3.3 (H3.3) and cleaved histone H3.3 at the T22 site (cH3.3) cDNA were cloned into the lentiviral vector pLV-SFFV-GFP (VectorBuilder). The lentiviral constructs, pLV-mH3 (5 μg) or pLV-mcH3 (5 μg), along with psPAX2 packaging plasmid (3.75 μg) and pMD2.G envelope plasmid (1.25 μg) were transfected into HEK-293T cells for virus package. The supernatant was collected at 48 h after the transfection. The viral particle containing supernatant was then used for the transduction of mH3.3 or mcH3.3 into 32D cells, a murine myeloblast-like cell line. The cells transduced of mH3.3 or mcH3.3 were used for CFU-C assay and Cell senescence assay after 1 week.

Chromatin immunoprecipitation (ChIP)

LK cells (2×10^6 for each condition) purified from BM of WT and *Brd4*^{Δ/Δ} mice were fixed with 1% formaldehyde for 15 min and quenched with 0.125 M glycine. Chromatin was isolated by the addition of lysis buffer, followed by shearing with Bioruptor Pico with water cooler (Diagenode, Seraing, Belgium). The DNA was sheared to an average length of 300–500 bp. Genomic DNA regions of interest were isolated using antibodies against H3 (Millipore Sigma, Cat#H0164) and cleaved Histone H3 (Thr22) (Cell Signaling, Cat#12576S). Complexes were washed, eluted from the beads with SDS buffer, and subjected to RNaseA and proteinase K treatment. Crosslinks were reversed by incubation overnight at 65°C, and ChIP DNA was purified using phenol-chloroform extraction and ethanol precipitation. After measuring DNA concentration with Qubit3.0, the DNA was used for qPCR. The primers used in ChIP-qPCR are shown in Appendix Table S2.

RNA sequencing

For RNA-seq of LSK cells, total RNA was isolated from WT and *Brd4*^{Δ/Δ} LSK cells with TRIzol reagent (Thermo Fisher, 15596018).

The RNA libraries were prepared followed by a stranded protocol with the KAPA UDI Adapter kit, and subjected to sequencing at a read length of paired-end 100 bp with final reads over 30 million per sample using the Illumina HiSeq 500. For RNA-seq of LK cells, total RNA isolated from WT and *Brd4^{Δ/Δ}* LK cells was subjected to RNA library preparation following a non-stranded protocol with the NEB Ultra RNA kit. All LK RNA-seq libraries were subjected to sequencing at a read length of paired-end 150 bp with final reads over 30 million per sample using the NovaSeq 6000. For all the sequenced data of LSK and LK cells, reads per sample were aligned to the mouse genome (GRCm38/mm10) using STAR (v2.7.0e) after being trimmed by Trimmomatic (v0.38). The raw read counts of each gene were calculated by HTSeq (v0.11.2). Then, the count matrix was used to identify differentially expressed genes by DESeq2 (LSK cells: FDR < 0.05 & |log₂ fold change| > 1; LK cells: FDR < 0.01 & |log₂ fold change| > 1). The transcripts per kilobase of exon model per million transcripts (TPM) matrix transformed by count matrix was used for gene set enrichment analysis (GSEA).

ATAC-seq

ATAC-seq was performed using WT and *Brd4^{Δ/Δ}* LK cells (50,000 cells) following the Omni-ATAC protocol (Corces *et al.*, 2017). Libraries were size selected for fragments at 100–700 bp with AMPure beads (0.56× and 1.8×), and paired-end sequencing was then performed on Nova-Seq (2 × 150 bp). Paired-end reads were aligned to the mouse reference genome (mm10) using Bowtie2 (v2.3.4.3) after being trimmed by TrimGalore (v0.5.0). PCR duplications were removed by Sambamba (v0.6.8). Reads with low mapping quality (< 30), reads mapped on mitochondria, or paired reads that are not on the same chromosome were filtered by Samtools (v1.9). The final bam files were then transformed to BED format by bedtools (v2.27.1). Peak calling was performed with MACS2 (v2.1.2) with options: -g mm --nomodel --shift -100 --extsize 200. The BAM files were normalized using deepTools (v3.1.3) to generate a BigWig file for visualization with options: --normalize Using CPM --binSize 50. Differential peaks were detected by DiffBind (Stark & Brown, 2011) (R/Bioconductor) with a threshold of FDR < 0.05. For transcription factor (TF) footprinting analysis, all peaks from each sample were merged by Homer, and the bam files were corrected for Tn5 insertion bias by TOBIAS (Bentsen *et al.*, 2020) (v 0.8.0) with the module of ATACCorrect. TF footprinting scores for each genotype were calculated by the FootprintScores module of TOBIAS (Bentsen *et al.*, 2020). The differential significance of TF footprinting levels was tested by the BINDetect module of TOBIAS. To explore the relationship between chromatin accessibility changes and gene dysregulation upon *Brd4* deletion, the correlation between fold changes in chromatin accessibility and gene expression level was calculated using cor.test with R. Fold change of the accessibility of each peak region was calculated by DESeq2 embedded within DiffBind. Fold change of each gene was calculated by DESeq2 with raw reads count matrix. Peak-related genes were determined by ChIPpeakAnno (R/Bioconductor).

Single-cell (sc) RNA sequencing and data analysis

LK and LSK cells were sorted from two mice of WT and *Brd4^{Δ/Δ}* cells. Individual samples were loaded on 10× Genomics

Chromium System aiming to generate 10,000 gel beads in emulsion (GEMs) per sample. scRNA-seq libraries were prepared according to the 10× Genomics protocol (Chromium Single Cell 3' Reagent kits User Guide V3 Chemistry). Libraries were sequenced on Illumina NovaSeq (paired-end), recovering a median of 400,000,000 reads/samples. Sequencing results (raw BCL format) from 10× Genomics of each library were demultiplexed and converted to FASTQ format by mkfastq module of cellranger (v3.0.2, 10× Genomics). For each library, the FASTQ data were aligned to the mouse reference genome (mm10/GRCm38) and further quantified by count module of cellranger with default parameters. Doublets were predicted by Scrublet (v0.2.1). The filtered results from cellranger and doublets prediction were imported into Seurat4 (Hao *et al.*, 2021) for downstream analysis. To ensure that the results are not affected by noise, the cells with low-quality and predicted doublets were excluded according to the following criteria: (i) with less than 500 or more than 6,000 detected features; (ii) with mitochondrial transcripts that accounted for more than 10% of the total detected transcripts; and (iii) predicted to be doublets by Scrublet. Genes that were detected in less than three cells for each sample were also excluded in the following analysis.

For LK scRNA-seq analysis, we finally obtained 11,586, 12,128, 13,304, and 13,711 cells for WT1, WT2, *Brd4^{Δ/Δ}*-1, and *Brd4^{Δ/Δ}*-2 separately. To eliminate the experimental and sequencing noise and identify the specific signaling associated with *Brd4* deletion, the unique molecular identifiers' counts were normalized, and the variable of mitochondrial transcript expression was repressed out for each sample separately with sctransform (v0.2.1). The normalized data from all four libraries were integrated with IntegrateData for downstream differential expression analysis. Principal component analyses (PCA) were performed on the scaled expression value of the top 3,000 highly variable genes (HVGs) for dimensionality reduction. Top 30 PCs were selected for sub-clusters detection, and uniform manifold approximation and projection (UMAP) was used to project all cells into two-dimensional space with resolution 1.0. Each cluster was then annotated according to the expression levels of known population-specific markers (Dahlin *et al.*, 2018; Giladi *et al.*, 2018).

Similarly, we performed scRNA-seq analysis on LSK cells. The cells with low-quality and predicted doublets and genes detected in less than three cells were removed from the dataset. A total of 6,968 (WT) and 7,626 (*Brd4^{Δ/Δ}*) LSK cells were retained for the analysis. After integrating two datasets and principal component analysis, the top 30 PCs were selected for sub-clusters detection, and UMAP was used to project all cells into two-dimensional space with resolution of 0.2. The cells with high expression of marker genes in mature cells were removed from the analysis. A total of 6,851 (WT) and 6,634 (*Brd4^{Δ/Δ}*) LSK cells were retained eventually for downstream analysis. Additionally, the retained immature cells were re-clustered (20 PCs, resolution 0.2) and annotated according to the expression levels of known HSPC markers (Tikhonova *et al.*, 2019).

Cleavage under target and release using nuclease (CUT&RUN) assay

CUT&RUN assay was performed according to the instruction of CUTANA ChIC/CUT&RUN Kit (SKU: 14-1048, EpiCypher). Briefly,

0.5 million sorted LK cells were incubated with activated Concanavalin A beads (Bangs Laboratories, BP531) and then incubated with antibodies against BRD4 (Active motif, 39909), H3K27ac (Diagenode, C15410174), H3K122ac (Abcam, ab33309), H3K4me3 (EpiCypher, 13-0041), H3K27me3 (EpiCypher, 13-0030) and Cleaved H3 (Cell Signaling, 12576S) at 4°C overnight. The cells were washed twice with Digitonin Buffer (20 mM HEPES, pH 7.5/150 mM NaCl, and 0.01% Digitonin) and incubated with pAG-MNase (EpiCypher) for 30 min followed by incubating with CaCl₂ (final concentration 2 mM) to activate digestion by pAG-MNase for 2 h at 4°C. The reaction was then stopped by adding the stop buffer (340 mM NaCl, 20 mM EDTA, 4 mM EGTA, 50 µg/ml RNase A, and 50 µg/ml glycogen) to each of the samples. The samples were then incubated in thermocycler (Bio-Rad) for 10 min at 37°C. The DNA was then purified using the DNA purification kit (NEB, T1030L) and subjected to Library preparation using NEBNext® UltraTM II Library Prep Kit for Illumina (Liu *et al*, 2018). Libraries were size selected with AMPure beads (Beckman) (0.8× and 1.2×) beads to generate libraries of 160–350 bp before paired-end sequencing was performed on a NextSeq 500 (35 bp).

Reads of each sample were aligned to the mouse reference genome (mm10) using bowtie2 (v2.3.4.3) after being trimmed by TrimGalore (v0.5.0). PCR duplications were removed by Sambamba (v0.6.8). Peak calling was performed by Homer with options: findPeaks Tagdirectory -style histone for histone modifications and -style factor for TFs. The BAM files were normalized using deepTools (v3.1.3) to generate a BigWig file for visualization with options: --normalize Using CPM --binSize 50. ChIPpeakAnno was used to annotate the total or differential peaks. To identify BRD4-binding regions across whole genome and eliminate non-specific binding of BRD4 antibody, significantly binding-reduced BRD4 peaks after *Brd4* deletion were selected from all peaks of WT LK cells by DiffBind using the embedded method DESeq2 with the threshold of FDR < 0.05.

Quantification and statistical analysis

GraphPad prism was used for all statistical analyses except RNA-seq, ATAC-seq, CUT&RUN, and single-cell RNA-seq datasets. Unless otherwise indicated, all individual values are shown on the graphs and statistical significance was determined by log-rank test, unpaired two-tailed Student's *t*-test, or one-way ANOVA followed by an appropriate *post hoc* correction. **P* < 0.05, ***P* < 0.01, ****P* < 0.001, and *****P* < 0.0001.

Data availability

The datasets produced in this study are available in the following databases: All sequencing and processed data have been submitted to the GEO archive (GSE189836). To review GEO accession GSE189836 (<https://www.ncbi.nlm.nih.gov/geo/query/acc.cgi?acc=GSE189836>), Bulk RNA-seq data: Gene Expression Omnibus GSE189834 (<https://www.ncbi.nlm.nih.gov/geo/query/acc.cgi?acc=GSE189834>), Single cell RNA-seq data: Gene Expression Omnibus GSE189835 (<https://www.ncbi.nlm.nih.gov/geo/query/acc.cgi?acc=GSE189835>), ATAC-seq data: Gene Expression Omnibus GSE189832 (<https://www.ncbi.nlm.nih.gov/geo/query/acc.cgi?acc=GSE189832>),

CUT&RUN data: Gene Expression Omnibus GSE189833 (<https://www.ncbi.nlm.nih.gov/geo/query/acc.cgi?acc=GSE189833>).

For each analysis performed, the software and version used are detailed in Appendix Table S4.

Expanded View for this article is available [online](#).

Acknowledgements

This work was supported by grants from the National Institutes of Health (HL149318 and HL158081 to F-CY, CA172408 and HL145883 to F-CY and MX, and CA240139 to SDN); Evan's foundation (to F-CY), NIH grant 1R01CA251698-01 and CPRIT grants RP180349 and RP190077 to C-MC, and the Leukemia and Lymphoma Society Specialized Center of Research grant (M1701632 to F-CY, MX, and SDN). GCCRI Genome Sequencing Facility/Mays Cancer Center Next-generation Sequencing Shared Resource/Biostatistics and Bioinformatics Shared Resource are supported by NIH-NCI P30 CA054174 (Cancer Center at UT Health San Antonio), NIH Shared Instrument grant 1S10OD021805-01 (\$10 grant), and CPRIT Core Facility Award (RP160732).

Author contributions

Hui Yang: Investigation; writing – original draft. **Pinpin Sui:** Data curation; writing – original draft. **Ying Guo:** Data curation. **Shi Chen:** Investigation. **Marie E Maloof:** Data curation. **Guo Ge:** Investigation. **Francine Nihozeko:** Investigation. **Caroline R Delma:** Investigation. **Ganqian Zhu:** Data curation. **Peng Zhang:** Investigation. **Zhenqing Ye:** Data curation. **Edward A Medina:** Writing – review and editing. **Nagi G Ayad:** Writing – review and editing. **Ruben Mesa:** Writing – review and editing. **Stephen D Nimer:** Supervision; writing – review and editing. **Cheng-Ming Chiang:** Writing – review and editing. **Mingjiang Xu:** Supervision; writing – review and editing. **Yidong Chen:** Data curation; writing – review and editing. **Feng-Chun Yang:** Project administration; writing – review and editing.

Disclosure and competing interests statement

The authors declare that they have no conflict of interest.

References

- Amorim S, Stathis A, Gleeson M, Iyengar S, Magarotto V, Leleu X, Morschhauser F, Karlin L, Roussais F, Rezai K *et al* (2016) Bromodomain inhibitor OTX015 in patients with lymphoma or multiple myeloma: a dose-escalation, open-label, pharmacokinetic, phase 1 study. *Lancet Haematol* 3: e196–e204
- Bansal H, Kornblau S, Qiu YH, Coombes KR, Panneerdoss P, Karnad A, Weitman S, Tomlinson G, Bansal S, Iyer SP (2017) Overexpression of BRD4 is an adverse prognostic factor in acute myeloid leukemia. *ASH Abstract* 130: 3794
- Bentsen M, Goymann P, Schultheis H, Klee K, Petrova A, Wiegandt R, Fust A, Preussner J, Kuenne C, Braun T *et al* (2020) ATAC-seq footprinting unravels kinetics of transcription factor binding during zygotic genome activation. *Nat Commun* 11: 4267
- Berthon C, Raffoux E, Thomas X, Vey N, Gomez-Roca C, Yee K, Taussig DC, Rezai K, Roumier C, Herait P *et al* (2016) Bromodomain inhibitor OTX015 in patients with acute leukaemia: a dose-escalation, phase 1 study. *Lancet Haematol* 3: e186–e195
- Cheung P, Schaffert S, Chang SE, Dvorak M, Donato M, Macaubas C, Foecke MH, Li TM, Zhang L, Coan JP *et al* (2021) Repression of CTSG, ELANE and PRTN3-mediated histone H3 proteolytic cleavage promotes monocyte-to-macrophage differentiation. *Nat Immunol* 22: 711–722

- Chiang CM (2009) Brd4 engagement from chromatin targeting to transcriptional regulation: selective contact with acetylated histone H3 and H4. *F1000 Biol Rep* 1: 98
- Corces MR, Trevino AE, Hamilton EG, Greenside PG, Sinnott-Armstrong NA, Vesuna S, Satpathy AT, Rubin AJ, Montine KS, Wu B et al (2017) An improved ATAC-seq protocol reduces background and enables interrogation of frozen tissues. *Nat Methods* 14: 959–962
- Dahlin JS, Hamey FK, Pijuan-Sala B, Shepherd M, Lau WWY, Nestorowa S, Weinreb C, Wolock S, Hannah R, Diamanti E et al (2018) A single-cell hematopoietic landscape resolves 8 lineage trajectories and defects in Kit mutant mice. *Blood* 131: e1–e11
- Dawson MA, Prinjha RK, Dittmann A, Giotopoulos G, Bantscheff M, Chan WI, Robson SC, Chung CW, Hopf C, Savitski MM et al (2011) Inhibition of BET recruitment to chromatin as an effective treatment for MLL-fusion leukaemia. *Nature* 478: 529–533
- Delmore JE, Issa GC, Lemieux ME, Rahl PB, Shi J, Jacobs HM, Kastiris E, Gilpatrick T, Paranal RM, Qi J et al (2011) BET bromodomain inhibition as a therapeutic strategy to target c-Myc. *Cell* 146: 904–917
- Dey A, Ellenberg J, Farina A, Coleman AE, Maruyama T, Sciortino S, Lippincott-Schwartz J, Ozato K (2000) A bromodomain protein, MCAP, associates with mitotic chromosomes and affects G(2)-to-M transition. *Mol Cell Biol* 20: 6537–6549
- Dey A, Yang W, Gegonne A, Nishiyama A, Pan R, Yagi R, Grinberg A, Finkelman FD, Pfeifer K, Zhu J et al (2019) BRD4 directs hematopoietic stem cell development and modulates macrophage inflammatory responses. *EMBO J* 38: e100293
- Donati B, Lorenzini E, Ciarrocchi A (2018) BRD4 and cancer: going beyond transcriptional regulation. *Mol Cancer* 17: 164
- Duarte LF, Young AR, Wang Z, Wu HA, Panda T, Kou Y, Kapoor A, Hasson D, Mills NR, Ma'ayan A et al (2014) Histone H3.3 and its proteolytically processed form drive a cellular senescence programme. *Nat Commun* 5: 5210
- Duncan EM, Muratore-Schroeder TL, Cook RG, Garcia BA, Shabanowitz J, Hunt DF, Allis CD (2008) Cathepsin L proteolytically processes histone H3 during mouse embryonic stem cell differentiation. *Cell* 135: 284–294
- Filippakopoulos P, Knapp S (2014) Targeting bromodomains: epigenetic readers of lysine acetylation. *Nat Rev Drug Discov* 13: 337–356
- Filippakopoulos P, Qi J, Picaud S, Shen Y, Smith WB, Fedorov O, Morse EM, Keates T, Hickman TT, Felletar I et al (2010) Selective inhibition of BET bromodomains. *Nature* 468: 1067–1073
- Gegonne A, Chen QR, Dey A, Etzensperger R, Tai X, Singer A, Meerzaman D, Ozato K, Singer DS (2018) Immature CD8 single-positive thymocytes are a molecularly distinct subpopulation, selectively dependent on BRD4 for their differentiation. *Cell Rep* 24: 117–129
- Giladi A, Paul F, Herzog Y, Lubling Y, Weiner A, Yofe I, Jaitin D, Cabezas-Wallscheid N, Dress R, Ginhoux F et al (2018) Single-cell characterization of haematopoietic progenitors and their trajectories in homeostasis and perturbed haematopoiesis. *Nat Cell Biol* 20: 836–846
- Gorgoulis V, Adams PD, Alimonti A, Bennett DC, Bischof O, Bishop C, Campisi J, Collado M, Evangelou K, Ferbeyre G et al (2019) Cellular senescence: defining a path forward. *Cell* 179: 813–827
- Hao Y, Hao S, Andersen-Nissen E, Mauck WM 3rd, Zheng S, Butler A, Lee MJ, Wilk AJ, Darby C, Zager M et al (2021) Integrated analysis of multimodal single-cell data. *Cell* 184: 3573–3587
- Itzen F, Greifenberg AK, Bosken CA, Geyer M (2014) Brd4 activates P-TEFb for RNA polymerase II CTD phosphorylation. *Nucleic Acids Res* 42: 7577–7590
- Iwasaki W, Miya Y, Horikoshi N, Osakabe A, Taguchi H, Tachiwana H, Shibata T, Kagawa W, Kurumizaka H (2013) Contribution of histone N-terminal tails to the structure and stability of nucleosomes. *FEBS Open Bio* 3: 363–369
- Jang MK, Mochizuki K, Zhou M, Jeong HS, Brady JN, Ozato K (2005) The bromodomain protein Brd4 is a positive regulatory component of P-TEFb and stimulates RNA polymerase II-dependent transcription. *Mol Cell* 19: 523–534
- Kim K, Punj V, Kim JM, Lee S, Ulmer TS, Lu W, Rice JC, An W (2016) MMP-9 facilitates selective proteolysis of the histone H3 tail at genes necessary for proficient osteoclastogenesis. *Genes Dev* 30: 208–219
- Lee JE, Park YK, Park S, Jang Y, Waring N, Dey A, Ozato K, Lai B, Peng W, Ge K (2017) Brd4 binds to active enhancers to control cell identity gene induction in adipogenesis and myogenesis. *Nat Commun* 8: 2217
- Lee M, Tayyari F, Pinnaduwa D, Bayani J, Bartlett JMS, Mulligan AM, Bull SB, Andrusis IL (2018) Tumoral BRD4 expression in lymph node-negative breast cancer: association with T-bet⁺ tumor-infiltrating lymphocytes and disease-free survival. *BMC Cancer* 18: 750
- Liu N, Hargreaves VV, Zhu Q, Kurland JV, Hong J, Kim W, Sher F, Macias-Trevino C, Rogers JM, Kurita R et al (2018) Direct promoter repression by BCL11A controls the fetal to adult hemoglobin switch. *Cell* 173: 430–442
- Loven J, Hoke HA, Lin CY, Lau A, Orlando DA, Vakoc CR, Bradner JE, Lee TI, Young RA (2013) Selective inhibition of tumor oncogenes by disruption of super-enhancers. *Cell* 153: 320–334
- Lu L, Chen Z, Lin X, Tian L, Su Q, An P, Li W, Wu Y, Du J, Shan H et al (2020) Inhibition of BRD4 suppresses the malignancy of breast cancer cells via regulation of Snail. *Cell Death Differ* 27: 255–268
- Mertz JA, Conery AR, Bryant BM, Sandy P, Balasubramanian S, Mele DA, Bergeron L, Sims RJ 3rd (2011) Targeting MYC dependence in cancer by inhibiting BET bromodomains. *Proc Natl Acad Sci U S A* 108: 16669–16674
- Midha A, Pan H, Abarca C, Andle J, Carapeto P, Bonner-Weir S, Aguayo-Mazzucato C (2021) Unique human and mouse beta-cell senescence-associated secretory phenotype (SASP) reveal conserved signaling pathways and heterogeneous factors. *Diabetes* 70: 1098–1116
- Ozer HG, El-Gamal D, Powell B, Hing ZA, Blachly JS, Harrington B, Mitchell S, Grieselhuber NR, Williams K, Lai TH et al (2018) BRD4 profiling identifies critical chronic lymphocytic leukemia oncogenic circuits and reveals sensitivity to PLX51107, a novel structurally distinct BET inhibitor. *Cancer Discov* 8: 458–477
- Penas C, Maloof ME, Stathias V, Long J, Tan SK, Mier J, Fang Y, Valdes C, Rodriguez-Blanco J, Chiang CM et al (2019) Time series modeling of cell cycle exit identifies Brd4 dependent regulation of cerebellar neurogenesis. *Nat Commun* 10: 3028
- Roe JS, Mercan F, Rivera K, Pappin DJ, Vakoc CR (2015) BET bromodomain inhibition suppresses the function of hematopoietic transcription factors in acute myeloid leukemia. *Mol Cell* 58: 1028–1039
- Saul D, Kosinsky RL, Atkinson EJ, Doolittle ML, Zhang X, LeBrasseur NK, Pignolo RJ, Robbins PD, Niedernhofer LJ, Ikono Y et al (2022) A new gene set identifies senescent cells and predicts senescence-associated pathways across tissues. *Nat Commun* 13: 4827
- Shi J, Vakoc CR (2014) The mechanisms behind the therapeutic activity of BET bromodomain inhibition. *Mol Cell* 54: 728–736
- Stark R, Brown G (2011) *DiffBind: differential binding analysis of ChIP-Seq peak data*. Cambridge: University of Cambridge
- Struhl K (1998) Histone acetylation and transcriptional regulatory mechanisms. *Genes Dev* 12: 599–606

- Tikhonova AN, Dolgalev I, Hu H, Sivaraj KK, Hoxha E, Cuesta-Dominguez A, Pinho S, Akhmetzyanova I, Gao J, Witkowski M et al (2019) The bone marrow microenvironment at single-cell resolution. *Nature* 569: 222–228
- Wang CY, Filippakopoulos P (2015) Beating the odds: BETs in disease. *Trends Biochem Sci* 40: 468–479
- Wu SY, Chiang CM (2007) The double bromodomain-containing chromatin adaptor Brd4 and transcriptional regulation. *J Biol Chem* 282: 13141–13145
- Wu SY, Lee AY, Lai HT, Zhang H, Chiang CM (2013) Phospho switch triggers Brd4 chromatin binding and activator recruitment for gene-specific targeting. *Mol Cell* 49: 843–857
- Yang Z, Yik JH, Chen R, He N, Jang MK, Ozato K, Zhou Q (2005) Recruitment of P-TEFb for stimulation of transcriptional elongation by the bromodomain protein Brd4. *Mol Cell* 19: 535–545
- Yang H, Kurtenbach S, Guo Y, Lohse I, Durante MA, Li J, Li Z, Al-Ali H, Li L, Chen Z et al (2018) Gain of function of ASXL1 truncating protein in the pathogenesis of myeloid malignancies. *Blood* 131: 328–341
- Zeng L, Zhou MM (2002) Bromodomain: an acetyl-lysine binding domain. *FEBS Lett* 513: 124–128
- Zuber J, Shi J, Wang E, Rappaport AR, Herrmann H, Sison EA, Magoon D, Qi J, Blatt K, Wunderlich M et al (2011) RNAi screen identifies Brd4 as a therapeutic target in acute myeloid leukaemia. *Nature* 478: 524–528